MECHANICAL ANALYSIS OF A GROWING CARBON NANOTUBE FOREST

A Thesis presented to

the Faculty of the Graduate School

at the University of Missouri-Columbia

In Partial Fulfillment

of the Requirements for the Degree Master of Science

---

by

DAMOLA M. AJIBOYE

Dr. Matthew R. Maschmann, Thesis Supervisor

DECEMBER 2016

The undersigned, appointed by the dean of the Graduate School, have examined the thesis titled:

Mechanical Analysis of a Growing Carbon Nanotube Forest

Presented by Damola M. Ajiboye,

a candidate for the degree of Master of Science,

and hereby certify that, in their opinion, it is worthy of acceptance.

_____

Professor Matthew R. Maschmann

_____

Professor Jian Lin

_____

Professor Stephen Montgomery-Smith

ACKNOWLEDGEMENT

With a deep sense of gratitude, I thank the Almighty God for bringing me thus far in my pursuit of academic excellence. Through these years, He has been my bedrock.

Also, I remain ever grateful to my advisor Dr. Matthew R. Maschmann whose patience and kind heartedness has helped nurture my intellectual pursuit. His consistent guidance and generosity in knowledge I must say has rubbed off on me.

Furthermore, I must also thank Dr. Jian Lin whose lectures further deepened my insight into the extraordinary world of the nanoscale. In addition, my immense gratitude goes to Dr. Stephen Montgomery-Smith whose strong mathematical lectures provided a strong foundation for my finite element studies.

Finally, my immeasurable thanks go to my parents who have persistently encouraged me to dream above my environments and see above circumstances that seem insurmountable.

Table of Contents

LIST OF FIGURES

LIST OF TABLES

ABSTRACT

Carbon nanotube forests are vertically oriented and entangled tubes that grow normal to a given substrate. The excellent thermal, mechanical, and electronic properties of individual carbon nanotubes motivates their study. Herein, two and three dimensional finite element models are developed to perform a mechanical analysis and parametric growth studies of actively growing carbon nanotube forests. Nanotube growth rate distribution, orientation angle, and diameter are varied to examine their effects on the resulting forest morphology. Individual carbon nanotubes are modeled as linear frame elements interconnected at adjacent nodes. The van der Waals interaction between carbon nanotubes is modeled as bar elements. The fastest-growing carbon nanotube in the forest are restricted by surrounding tubes, thereby generating a compressive force that is transmitted to the base of the carbon nanotube. The slowest growing carbon nanotube transmits tensile forces. The simulated forest morphology exhibits a strong consistency with observed carbon nanotube forests whilst maintaining mechanical phenomena like buckling, translation and rotation as seen in electron micrographs. This modeling approach is a paradigm shift in the study of carbon nanotube forest growth mechanics and establishes a framework for further thermal and electrical analyses.

Chapter 1 Introduction

1.1 Introduction

The progress of civilization overtime has showed a strong correlation with the discovery of novel materials which serve as a catalyst in reaching previously unattainable heights in human development[1]. This is quite consistent with earlier civilizations which were rightly marked by their respective levels of materials development (Stone Age 2.5 million BC, Bronze Age 3500 BC and Iron Age 1000 BC. The recent developments in the science of the nanoscale has ushered in the discovery of carbon nanotubes (CNT) which has showed tremendous promise in technological applications ranging from biotechnology[2], energy storage[3, 4], composite materials[5], electronics[6, 7], microelectronics[8, 9], optics[10, 11], hydrogen storage[12, 13], solar energy[14], thermal management[15] and other applications.

1.11 Brief History of the Discovery of Carbon Nanotubes

Credit for the discovery of carbon nanotubes is quite a controversial issue with the current literature blindly ignoring the previous works of a plethora of scientists in this field.

Without a doubt one must acknowledge the impact of Iijima's 1991 publication[16] in this field but that is not to say that carbon nanotubes have not been seen previously in the literature.

Carbon nanotubes as we know were first reported in 1952 by Radushkevich et al. in the Journal of Physical Chemistry of Russia [17] but due to the inaccessibility of the

Russian language by western scientists and the prevailing political conditions of the cold war, this discovery went unnoticed in the west. The reported images from the journal in question [17] clearly showed the tubular structure of carbon nanotubes with clear indications of its nanoscale and multiwalled structure. This publication was followed by numerous contributions by notable scientists in the field of carbon namely Oberlin, Baker, Baird, Endo, Harris, Robertson, Walker[18] et cetera. Furthermore, it must be noted that the due to the limitations of the then available transmission electron microscopes, the presence and arrangement of graphene in the carbon nanotube images could not be identified.

In spite of these previous discoveries of carbon nanotubes, one cannot deny the immense traction gained by Iijima's 1991 rediscovery of carbon nanotubes. This can be ascribed to the relative top rank of the publishing journal (NATURE). Also, the availability of comparatively sophisticated tools for materials characterization along with the renewed interest in the nanoscale played a big role in advancing the reach of this work [18].

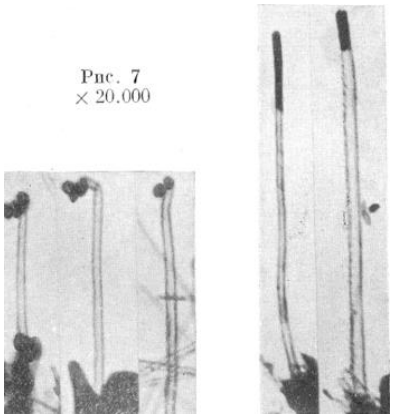

Figure 1.1 Transmission electron microscope images of carbon nanotubes presented by Raduskevich et al [17].

1.2 Structure of Carbon Nanotubes

Carbon nanotubes primarily exist in a single-walled and multiwalled state as shown below where the single-wall carbon nanotube is a hollow tube comprising of carbon atoms with diameters ranging from 0.5nm to 5nm and with length ranging from a few micrometers to centimeters [19]. The multiwall carbon nanotube consists of multiple nested walls with spacing in the region of 0.34nm.

In order to reveal the physical structure and electronic band structure of carbon nanotubes, the concept of chirality is employed. The concept of chirality is used to describe reflection symmetry between an object and its mirror image. That is to say, a chiral image is not superimposable on its mirror image in contrast to an achiral image which is superimposable. Single wall carbon nanotubes can be classified into:

a) Chiral carbon nanotube

b) Armchair carbon nanotube

c) Zigzag carbon nanotube

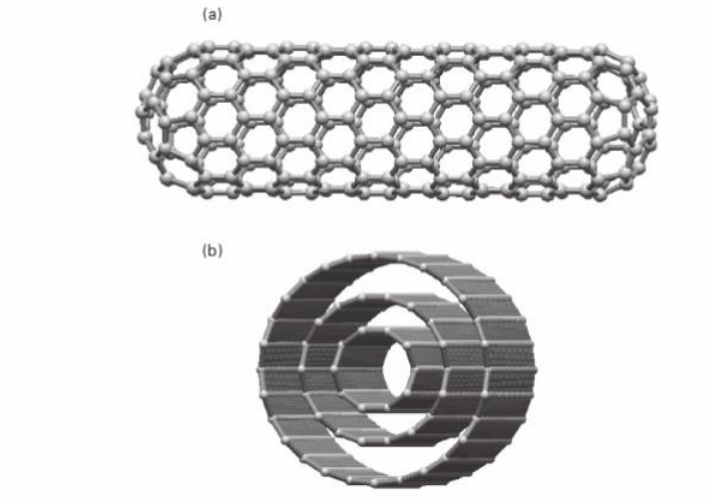

Figure 1.2 Diagrammatic representation of carbon nanotubes: (a) single wall carbon nanotube (b) multiwall carbon nanotube [19].

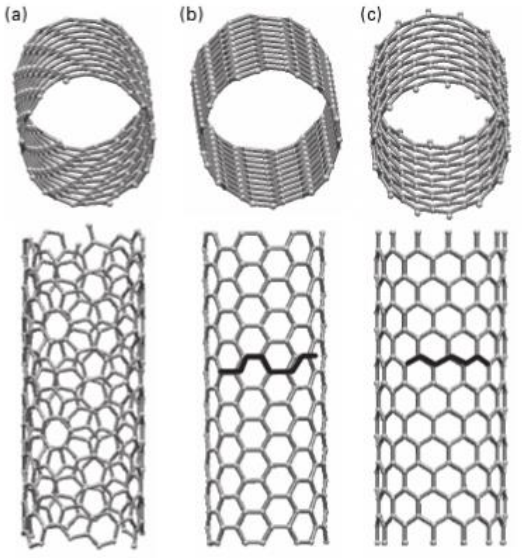

Figure 1.3 Illustration of the various types of single-wall carbon nanotube: a) chiral carbon nanotube b) armchair carbon nanotube c) zigzag carbon nanotube [19].

The structure of the cylindrical carbon nanotube is a result of folding or wrapping a graphene sheet which can be described mathematically with primitive lattice vectors as given below:

$$a_1 = \left[\frac{\sqrt{3}a}{2}, \frac{a}{2}\right] a_2 = \left[\frac{\sqrt{3}a}{2}, -\frac{a}{2}\right] \textbf{[1.1]}$$

where **a** is the bravais lattice constant which equals 2.46 Angstrom.

The above mathematical description of graphene provides exact information for the derivation of the primitive lattice of carbon nanotubes which is paramount in the description of its CNT band structure. The images in Figure 1.4 below show the honeycomb lattice of graphene and the corresponding primitive lattice vectors. For the holistic description of a carbon nanotube, three fundamental parameters are employed:

a. Chiral vector C_h (or circumferential vector)

b. Translation vector T

c. Chiral angle θ

The chiral vector is employed in describing the CNT geometrically where C_h is the modulus of the circumference and it is also known to connect any two primitive lattice points of graphene. Furthermore, chiral vector values are good indicators of the type of carbon nanotubes considered where a chiral vector of **(n, n)** indicates an armchair nanotube, (**n, 0)** connotes a zigzag nanotube and all other forms like **(n, m)** indicate a chiral nanotube.

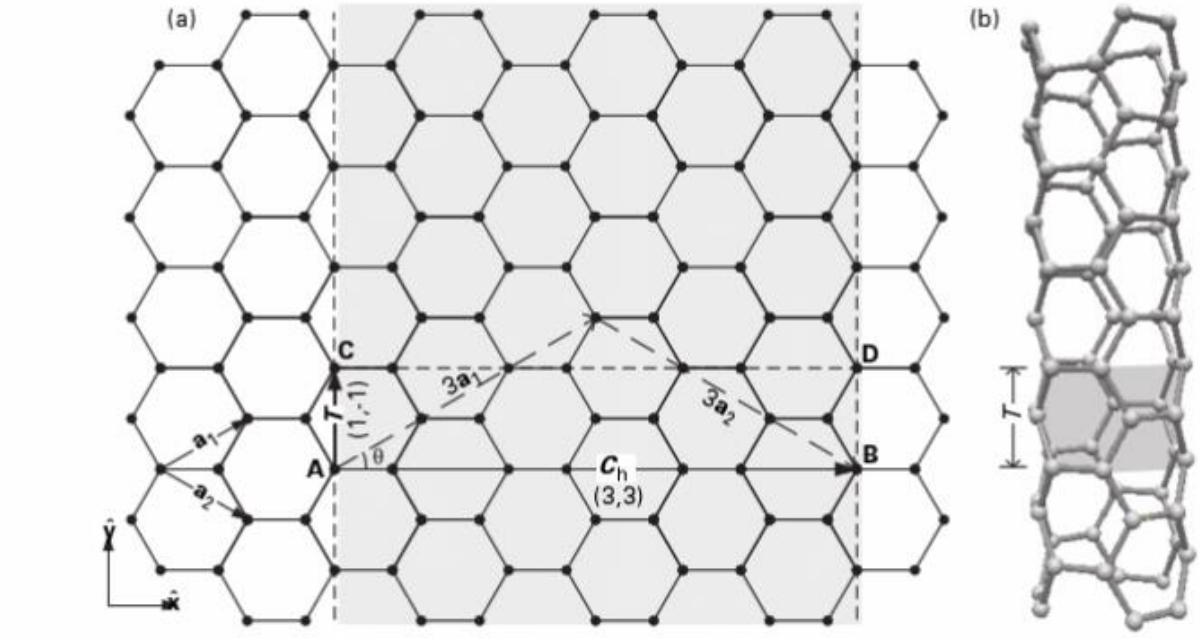

Figure 1.4 Carbon nanotube from graphene. (a) Folding of the dashed lines containing points A and C to those passing through points B and D gives a (3,3) armchair carbon nanotube seen in (b). Result shows the primitive unit cell. [19]

The diameter d_t of a carbon nanotube can be derived from the modulus of its circumference $|C_h|$

$$d_t = \frac{|C_h|}{\pi} = \frac{\sqrt{C_h \cdot C_h}}{\pi} = \frac{a\sqrt{n^2 + nm + m^2}}{\pi} \quad \textbf{[1.2]}$$

It is quite interesting to note that CNTs with different chiralities can produce the same diameter.

Table 1.1.1 Parameters associated with carbon nanotubes [19].

Symbol	Name	cCNT	aCNT	zCNT
$\boldsymbol{C}_\mathrm{h}$	chiral vector	$\boldsymbol{C}_\mathrm{h} = n\mathbf{a}_1 + m\mathbf{a}_2 = (n,m)$	$\boldsymbol{C}_\mathrm{h} = (n,m)$	$\boldsymbol{C}_\mathrm{h} = (n,0)$
C_h	length of chiral vector	$C_\mathrm{h} = \lvert C_\mathrm{h}\rvert = a\sqrt{n^2 + nm + m^2}$	$C_\mathrm{h} = a\sqrt{3}n$	$C_\mathrm{h} = an$
d_t	diameter	$d_\mathrm{t} = \frac{a}{\pi}\sqrt{n^2 + nm + m^2}$	$d_\mathrm{t} = \frac{an}{\pi}\sqrt{3}$	$d_\mathrm{t} = \frac{an}{\pi}$
θ	chiral angle	$\cos\theta = \frac{2n+m}{2\sqrt{n^2+nm+m^2}}$	$\theta = 30°$	$\theta = 0°$
g_d	greatest common divisor	$g_\mathrm{d} \equiv \gcd(2m+n, 2n+m)$	$g_\mathrm{d} = 3n$	$g_\mathrm{d} = n$
$\boldsymbol{T}$	translation vector	$T = \frac{2m+n}{g_\mathrm{d}}\mathbf{a}_1 - \frac{2n+m}{g_\mathrm{d}}\mathbf{a}_2$	$\boldsymbol{T} = \mathbf{a}_1 - \mathbf{a}_2$	$\boldsymbol{T} = \mathbf{a}_1 - 2\mathbf{a}_2$
T	length of translation vector	$T = \lvert T\rvert = \frac{\sqrt{3}C_\mathrm{h}}{g_\mathrm{d}}$	$T = a$	$T = a\sqrt{3}$
N	number of hexagons/cell	$N = \frac{2C_\mathrm{h}^2}{a^2 g_\mathrm{d}}$	$N = 2n$	$N = 2n$

1.3 Properties of Carbon Nanotubes

1.31 Mechanical Properties of Carbon Nanotubes

The exceptional mechanical properties of carbon nanotubes have been well lauded, these properties include the capacity to sustain large elastic strain, high fracture strength, and high elastic modulus et cetera.

Overtime, extensive work has been done in elucidating the mechanical properties of single-walled carbon nanotubes. Overney et al. [20] investigated the rigidity and low-

frequency vibration of carbon nanotubes made up of 100-400 atoms using the Keaton Hamiltonian approach. Herein, a comparison was made between an iridium beam and the bending stiffness of single-walled nanotubes wherein they concluded that the bending stiffness of carbon nanotube supersedes those of any other material ever known to man [20].

Iijima et al. [21] also studied the mechanical properties of carbon nanotubes albeit with a theoretical and experimental approach. Here they approached the study using the molecular dynamics method where the properties of carbon nanotubes under compression were probed. Their results showed the excellent flexible properties of carbon nanotubes and remarkable resistance to large strains as revealed in figure 1.5 below.

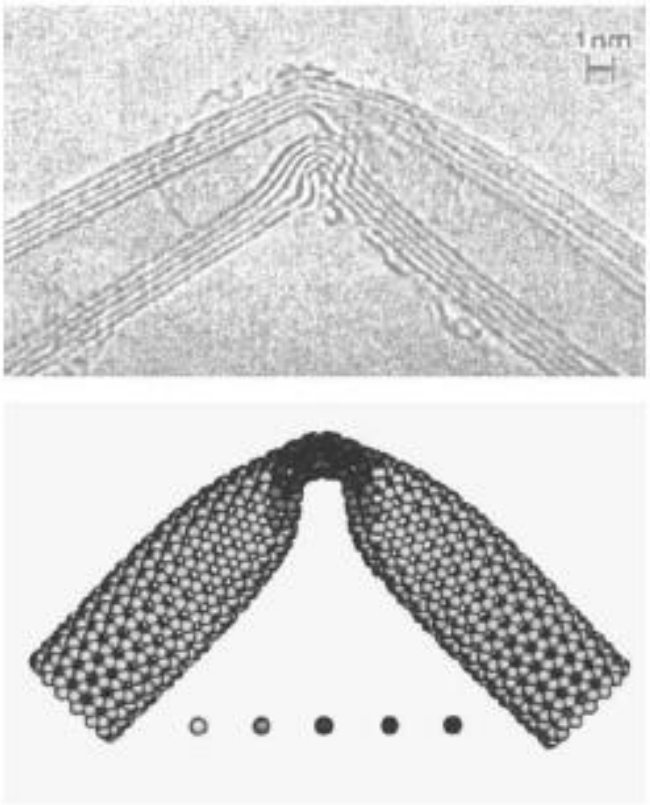

Figure 1.5 Transmission electron microscope micrograph and molecular dynamics results showing buckling of carbon nanotubes [21].

In addition to these studies, Vaccarini et al. [22] investigated the relationship between nanotube structures and chirality on their elastic properties in bending, tension, and torsion. They concluded that the influence of chirality on the tensile modulus was minimal. Also it was noticed that chiral tubes exhibit a non-symmetrical torsional behavior with respect to left and right twist, as opposed to armchair and zigzag tubes where this behavior is absent.

Aside the exceptional elastic properties of carbon nanotubes, the inelastic behavior of carbon nanotubes have also been noted. Yakobson et al. [23] studied the response of carbon nanotubes beyond the elastic limit. This was investigated by employing the Tersoff-Brenner potential in tandem with molecular dynamics simulations. Their work showed that carbon nanotubes under large deformation revert to different morphological patterns where

each shape signifies an instantaneous release of energy in the stress/strain curve. In addition, Yakobson et al.,[24]applied the dislocation theory to carbon nanotubes to characterize their routes of mechanical relaxation under tension. Their results showed that the yield strength of carbon nanotubes depends on its symmetry where it is believed that there exists an intra-molecular plastic flow. In the presence of high stress, the plastic flow corresponds to a motion of dislocations along helical paths which cause stepwise necking.

1.32 Electrical Properties of Carbon Nanotubes

It is well documented that carbon nanotubes with high aspect ratio possess excellent electrical conductivity. This property of carbon nanotubes suggests that with a little addition into dispersed polymers, one could produce nanocomposites with a very high electrical conductivity. Along the longitudinal axis, carbon nanotubes are either metallic or semiconductors with their conductivity depending on the chiral vector (n, m). If n equals m, the carbon nanotube is said to be metallic, on the other hand if the result of n minus m is a multiple of three, the carbon nanotube will be a semiconductor. The exception to this rule arises in the presence of curvature effects which strongly influence its electrical properties.

Hu et al. based on theoretical and experimental methods studied the electrical properties of CNT/polymer nanocomposites[25]. Using the statistical percolation theory, a three dimensional (3D) numerical model was developed to approximate the electrical properties of a nanocomposite which was made from insulating polymers filled with carbon nanotubes.

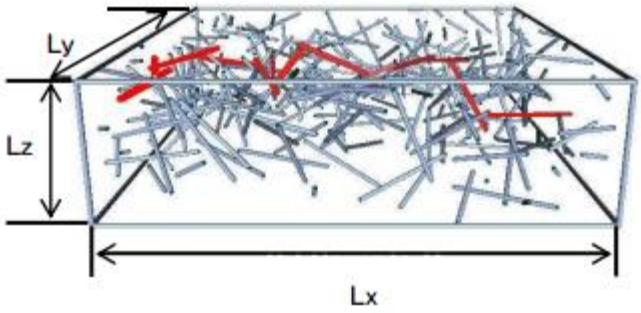

Figure 1.6 Diagrammatic representation of a three dimensional element with haphazard dispersion of carbon nanotubes [25].

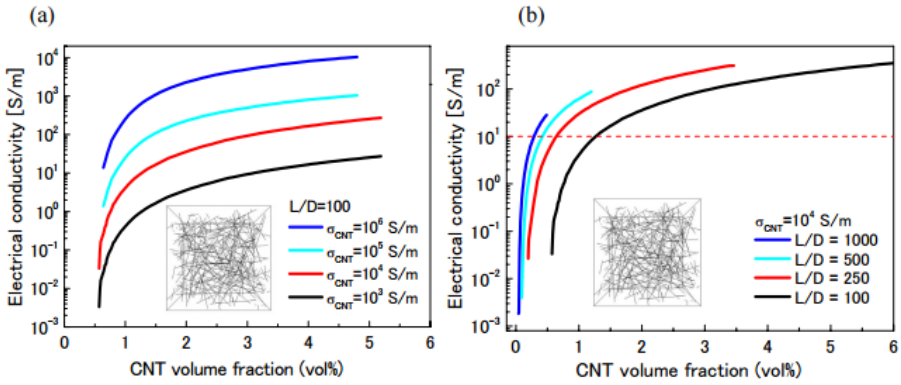

Figure 1.7 Effects of (a) the electrical conductivity (b) aspect ratio of individual carbon nanotubes on the electrical conductivity of nanocomposites [25].

Their numerical results showed a strong correlation with experimental data especially for relatively high CNT volume fraction. As shown in figure 1.7a above, the electrical conductivity of individual carbon nanotubes greatly enhances the electrical conductivity of nanocomposites. It was also seen that for carbon nanotubes with less curvature (straight nanotubes), the electrical conductivity of the nanocomposite is proportional to the conductivity of the individual nanotubes. In addition, high aspect ratio of carbon nanotubes was also seen to translate to excellent electrical conductivity. This portends that carbon nanotubes with high aspect ratio will be suitable as fillers for achieving high electrical conductivity in various industrial applications.

1.33 Thermal Properties of carbon nanotubes

The lauded thermal properties of carbon nanotubes are a direct consequence of their nanoscale size and their unique structure. It is well known that the specific heat of single-walled nanotubes differs from those of two-dimensional graphene and 3-D graphite. This is even more pronounced at low temperatures where the 1-D quantization of the band structure is prevalent.

The demand for miniaturized high-tech electronic devices in recent years precipitates intense research in the thermal management of nanoscale and microscale systems. The unique electronic properties have long been known with its conductivity (i.e. metallic or semiconductor) heavily dependent on its chirality. Che et al [26] studied the thermal conductivity of carbon nanotubes using a molecular dynamics simulation which incorporates the theoretical fluctuation-dissipation relation.

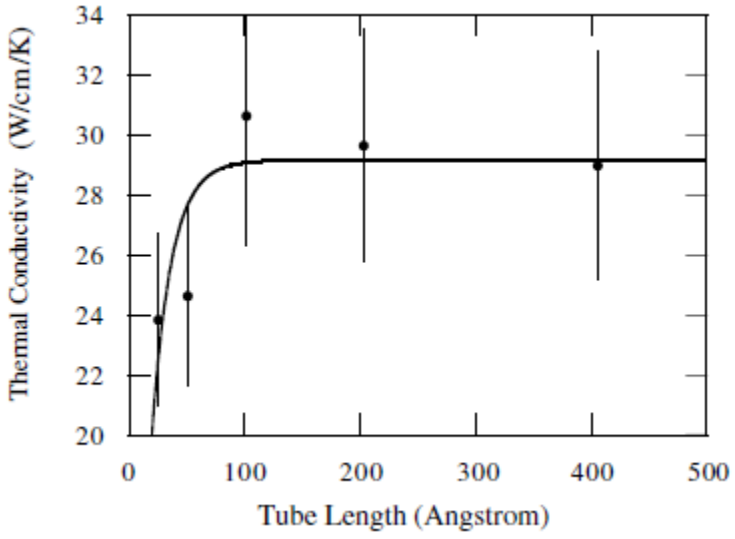

Figure 1.8 Dependence of thermal conductivity on the length scale of nanotubes [26].

For validation of thermal results, convergence of the molecular dynamics approach was tested using an array of systems with different size (systems with 400, 800, 1600, 3200, 6400 atoms). Here it was observed that the phonon mean free path was an obstacle to accuracy especially in smaller scales. But with increase in the scale of the system, so do the theoretical values approach a threshold that is independent of size as seen in figure 1.8 above.

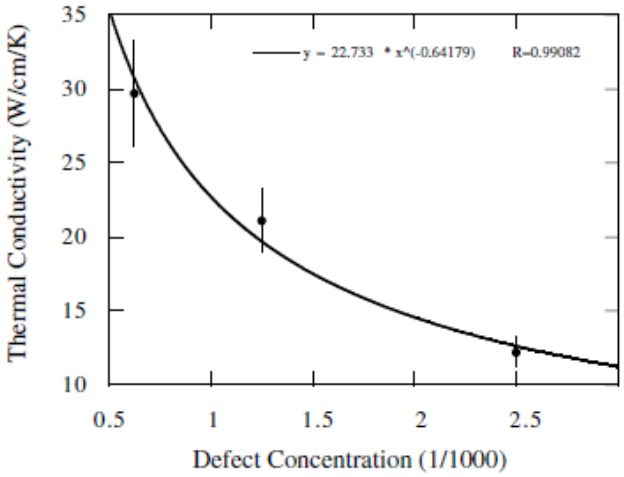

Figure 1.9 Thermal conductivity as a function of defect concentration [26].

These high thermal conductivity values are true only for defect free carbon nanotubes hence the investigation of the effects of defects and vacancies on thermal conductivity of carbon nanotubes as seen in figures 1.9 and 1.10.

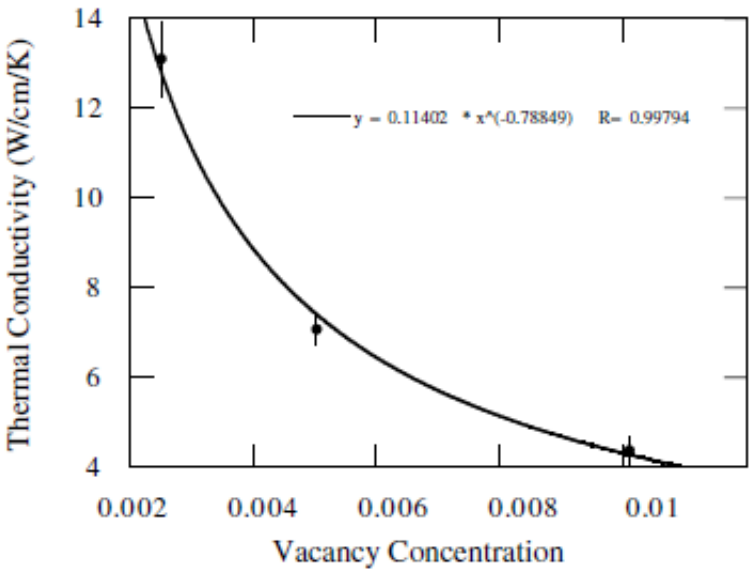

Figure 1.10 Relationship between thermal conductivity and vacancy concentration [26].

1.4 Potential applications of carbon nanotubes

1.4.1 Composite Materials

In industry, the use of carbon nanotubes as components of composite materials is gaining popularity[27]. Multiwalled carbon nanotubes have found application as electrically conductive fillers in plastics, essentially making use of their high aspect ratio in order to form a percolation network at concentrations as low as 0.01 weight percent (wt%).

In the automotive industry, conductive carbon nanotube plastics have found applications in fuel lines, filters that dissipate electrostatic charge and electrostatic painting of mirror housings. For structural application, stiffness, strength and toughness is greatly improved by the mixing of carbon nanotube powders with polymers. For example, addition of ~1wt% multiwalled nanotube to epoxy resin improves stiffness and fracture toughness by 6 and 23% respectively. Furthermore, CNTs and CNT polymer contacts have been seen to greatly improve material damping which is employed in sporting equipment like

baseball bats, bicycle frames and tennis racquets. Also, it has been reported that addition of minute amounts of CNTs to metals improves their tensile strength and modulus.

In conclusion, multiwalled carbon nanotubes can also be used as flame retardant additive to plastics [28] which is largely due to changes in rheology by nanotube loading. These plastic applications will serve as an attractive replacement for halogenated flame retardants which are known to have adverse environmental effects. Below in figure 1.11 are images showing the present day use of carbon nanotubes in structures.

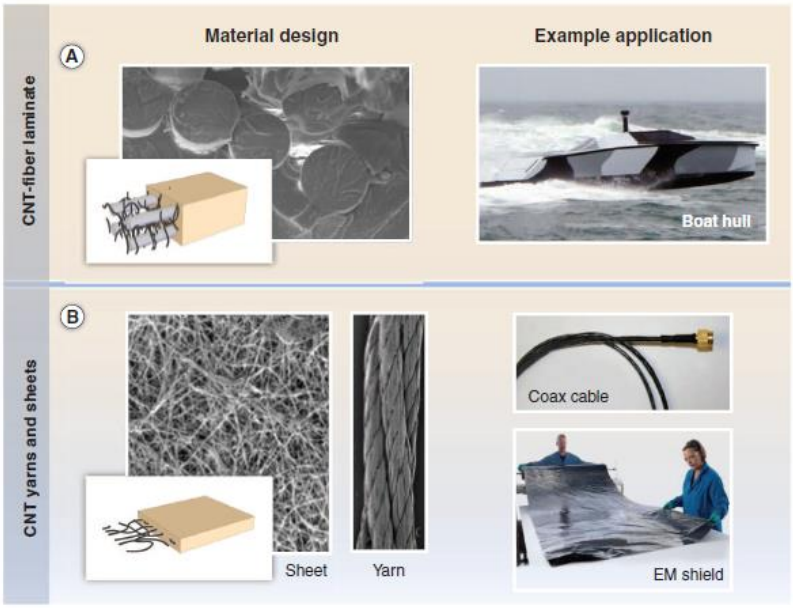

Figure 1.11 Applications of carbon nanotube composites and macrostructures. (A) Carbon fiber laminate cross section with dispersed carbon nanotubes and a carbon nanotube-fiber enhanced boat hull. (B) Electromagnetic (EM) shielding materials from nanotubes [27].

1.4.2 Microelectronics

The application of high quality single walled nanotubes in transistors is quite feasible due to their low electron scattering and their bandgaps. Great strides have been made in the application of carbon nanotubes as microelectronic devices, for example in 1998 the first

carbon nanotube transistor was manufactured. Some years later, the first single walled nanotube tunneling field effect transistor (FET) and carbon nanotube based radios were manufactured. As recent as 2012, single walled nanotube FETs with sub 10nm channel lengths showed a current density which supersedes those employed in present day silicon devices. In spite of these tremendous potentials for single walled carbon nanotube devices, control of carbon nanotube diameters, chirality, and density still remains an impediment to large scale production.

As a result of their low scattering, high current carrying capacity, carbon nanotubes have been suggested to replace Cu in microelectronic interconnects. Also, carbon nanotubes have been known to be able to function as electrical loads and heat dissipaters which make them potential alternatives to solder bumps.

1.4.3 Coatings

The application of multiwalled carbon nanotubes in paint has been shown to reduce of ship hulls. This is achieved by carbon nanotubes acting as an obstruction to the attachment of algae and barnacles. Also, addition of carbon nanotubes to anticorrosive coatings can potentially improve the stiffness and strength whilst creating a pathway for cathodic protection [29].

1.4.4 Films

The high cost of indium tin oxide due to its high demand in flexible displays, touch screen devices, photovoltaic serves as incentive to its replacement by carbon nanotubes. In addition to cost, it's comparatively easy processing methods (slot-die coating, ultrasonic spraying) make carbon nanotubes excellent alternative to indium tin oxide [30].

1.4.5 Biotechnology

The compatibility of carbon nanotubes with biomolecules as pushed for its use in biosensors and medical appliances. Such devices include microscopic arrays for protein and DNA detection, and biosensors for toxin and gas detection. Furthermore, it has been well documented that carbon nanotubes can be internalized by cell membranes thereby paving way for in vivo application [31]. The drawback to its full integration in bio products remains concerns about toxicity. Although it has been argued that its inherent geometry and surface chemistry greatly affects biocompatibility thus this property could be engineerable [32].

1.4.6 Probes

The mechanical robustness and low buckling force of CNTs have informed its use in scanning probe tips for atomic probe microscopes (figure 1.12). Its geometry (cylindrical shape) and minute tube circumference allows for imaging inaccessible nooks and crannies of examined specimens [33]. In addition, use of biological ligands on CNT nanoprobes allows for the mapping of chemical and biological functions of condensed samples[34]. Lastly, nanoscopic tweezers from CNTs have showed promise in their use as nanoprobes for assembly.

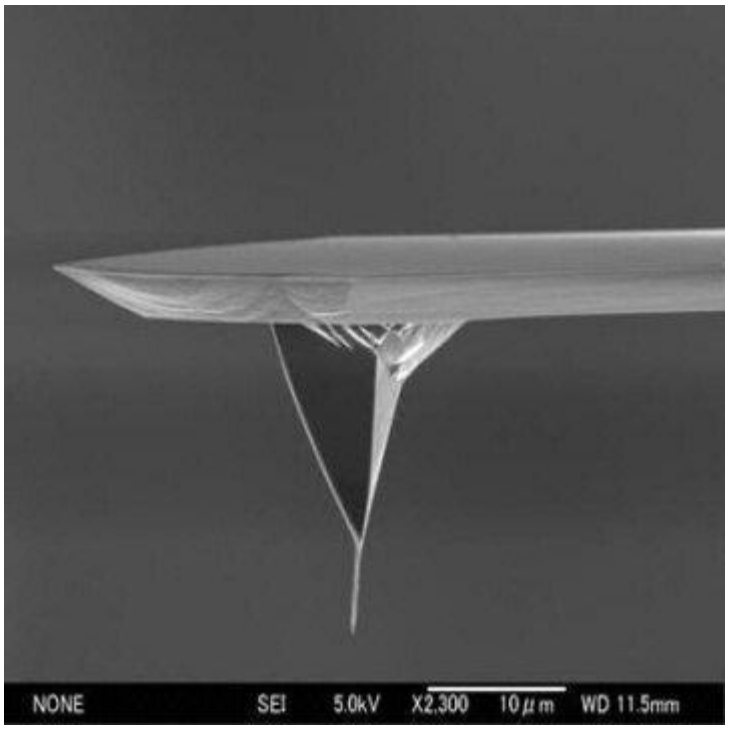

Figure 1.12 Micrograph of carbon nanotube based atomic force microscope probes.

1.4.7 Field Emission Devices

Extensive research in electronic devices has primarily concentrated in the use of carbon nanotubes as a source of field emission electrons which are employed in lamps, gas discharge tubes, x-ray [35] and microwave generators. It is well known that a potential applied between a carbon nanotube surface and an anode produces a considerable high local field which is primarily due to the minute radius and length of the fibers. The influence of the local fields causes electrons to tunnel directly from the nanotube tip into the vacuum. The total effect of the electric field is seen in the direction of the field-emitted electrons in the direction of the anode, where a phosphor produces light for the flat panel display application as seen in figure 1.13. The ease of manufacturing nanotube field-emitting surfaces by screen-printing has further fueled the call for its use as replacements of tungsten and molybdenum tip arrays which are more difficult to fabricate.

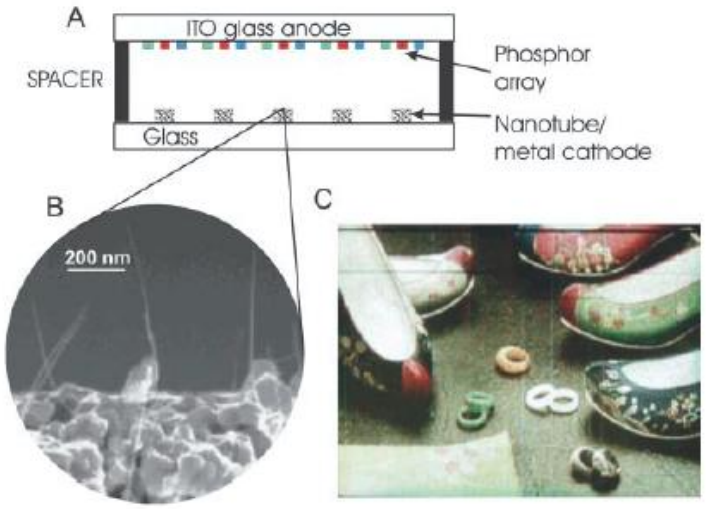

Figure 1.13 (A) Schematic of a carbon nanotube based flat panel displays (B) Scanning electron micrograph of an electron emitter for displays. (C) Example of image produced by field emission display [36].

Chapter 2 Time Resolved Modeling of a Growing Carbon Nanotube Forest

2.1 Introduction

The rediscovery of carbon nanotubes in 1991 heralded the beginning of a new phase in materials science. This laudatory appraisal is mainly due to its exceptional thermal, electronic, mechanical and electronic properties [4]. These properties has exhibited by carbon nanotubes make them ideal for electrical interfaces [36], vias [37], thermal interfaces[38], mechanical sensors [39, 40]. Considering that extensive research and resources [27] has gone into the understanding of these materials, little work has been done in unraveling the influence of inter carbon nanotube interactions on the forest morphology.

Mechanical modeling offers a new frontier for the study of the underlying phenomena that occurs in a growing carbon nanotube forest. In the literature, work has been done in this area albeit with significant physical idealizations. For example, carbon nanotubes have been modeled has vertical and non-interacting beams [41, 42], isotropic and homogeneous solids [43], and individual unit cells made of neighboring carbon nanotubes in contact [44, 45]. Considering the complexity of carbon nanotube forests, high degree of anisotropy, tortuosity and inhomogeneity, these models fail to capture the inherent processes that are embedded therein. Also, they provide limited guidance and applicability in terms of the wide range of carbon nanotube morphologies. Finally, they fail to capture the phenomenon of carbon nanotube growth in real time since their results are collected only after completion of growth. Due to these significant idealizations, the ability to quantitatively predict the carbon nanotube forest growth mechanics and anticipate changes to its morphology as a result of changes in growth parameters is lacking.

Carbon nanotubes within a given forest are characterized by distributed growth parameters that include surface area, growth rate, diameter, catalyst lifetime and diffusion rate. With growth, the spatial density and relative alignment of carbon nanotube forests may be highly variable as a function of forest height as interactions between neighboring carbon nanotubes change with time. Previous works have been carried out in the spatial characterization carbon nanotube forests with consideration given to the carbon nanotube density, alignment, and diameter distribution using small angle x-ray scattering (SAXS)[44, 46, 47].

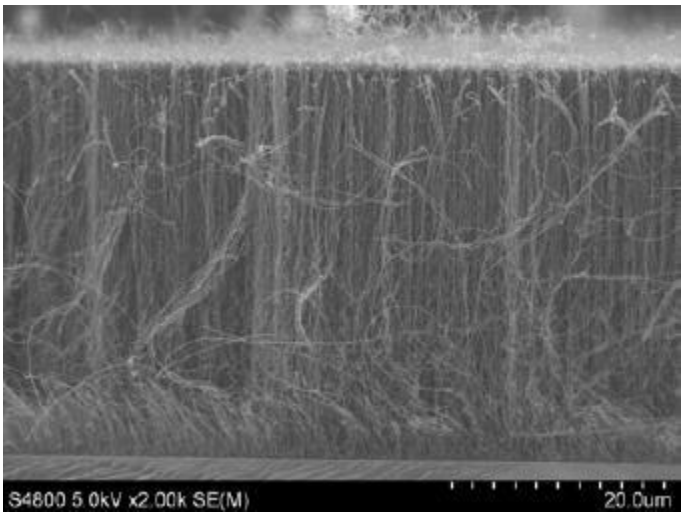

Figure 2.1 Scanning Electron Microscope micrograph of a carbon nanotube forest.

Carbon nanotube forests exhibit anisotropic behavior due to their preferred growth orientation [48, 49]. Recent reports have showed that the stiffness anisotropy of carbon nanotubes in the axial and transverse directions differ by approximately two orders of magnitude[49]. The literature is abound with studies on the anisotropic behavior of carbon nanotube forests after synthesis but lacking in understanding the processes and interactions that underlie this forests during growth. The implication of a model with the capacity to

monitor growth on the fly is that mechanical, chemical, electrical and thermal properties could be predicted with a comprehensive understanding of the occurring physics in the carbon nanotube forest.

In this work, a finite element model is presented to study the physics of carbon nanotube growth. The given finite element model is also capable of mechanical, electrical, thermal and potentially chemical analyses of a carbon nanotube forest. Herein, the finite element model accepts distributed parameters such as carbon nanotube growth rate, orientation relative to the substrate, outer diameter, inner diameter, spatial density, elastic modulus, and shear modulus. With these input parameters, the model outputs a time-resolved evolution of carbon nanotube morphology. This is done through end-to-end addition of plane frame elements at discrete time steps to obtain a single standing carbon nanotube. Also, the van der Waals force found in carbon nanotube forests are modeled as linear elastic bar elements wherein they are introduced only after the nodes of nanotubes in close proximity surpass a predetermined target distance. After which the contacting carbon nanotubes are allowed to rotate, translate, and buckle based on the arising reaction forces due to differing growth rates and orientations. The resulting carbon nanotube forest is quite consistent with experimentally observed forests with all attributes as seen in electron micrographs also repeating in the model plots.

2.2 Experimental Procedure

The growth sequence of the carbon nanotube forest begins with the nucleation phase where the fundamental properties of the forest are established for all nanotubes. Herein, individual carbon nanotubes are assigned to specific nucleation sites and given growth rates and orientation angles which will persist to the very end of the growth sequence. In addition to

this, the inner diameter, outer diameter, elastic modulus and modulus of rigidity are also assigned to individual nanotubes in this phase. The assignment of these properties to forest nanotubes is solely based on user-defined distributions. For this work, a forest of 100 uniformly spaced carbon nanotubes on a 10μm substrate is employed. The average growth rate for the carbon nanotube forest is computed as 75nm/step whilst growing the forest population at an average orientation angle of 90° (normal to the substrate). The employed standard deviation of these variables is arrived upon based upon a percentage of the average values. The programmed growth rate distributions include standard deviations of 5%, 10%, and 20% of the established average value. Furthermore, the angular orientation of individual nanotubes is given standard deviations of 5%, 10%, and 20% of the mean value. Also considered are the outer diameters of 5, 25 and 50nm where the inner diameter is scaled to 60% of the outer diameter in each distance. In terms of geometry, the carbon nanotubes are modeled as hollow cylinders with solid walls.

Nucleation of a carbon nanotube forest is executed by the introduction of the plane frame elements to the pre-assigned nucleation sites whilst tilted at the given orientation angles. Plane frame elements are 1-D finite elements with a total of six degrees of freedom per element. Each node allows for an axial displacement u, transverse displacement v and rotation Θ as shown in figure 2.2. The nucleation phase is programmed to occur simultaneously for all nanotubes in the forest. The subsequent growth steps will involve pushing the initial growth segments upward in a manner similar to the base growth mechanism of synthesizing carbon nanotubes

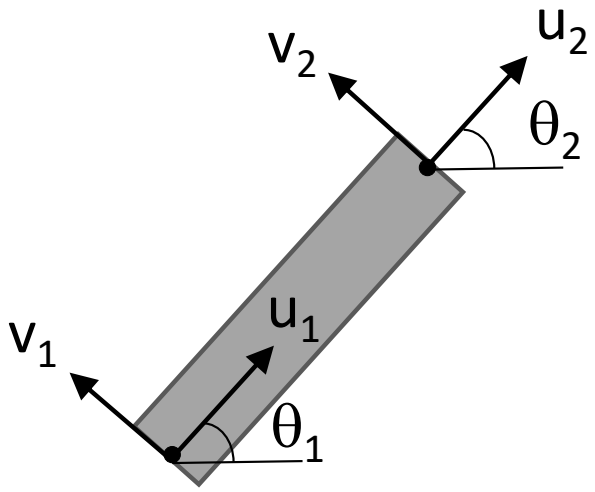

Figure 2.2 Plane frame element employed to model a carbon nanotube forest, where u (axial displacement), v (transverse displacement), and θ (rotation) are located at each of the endpoints nodes.

The nucleation phase is followed by the computation of the 6 x 6 local stiffness matrix of each carbon nanotube wherein the stiffness influence coefficients correspond to the axial, transverse and rotational degrees of freedom as seen in Figure 2.2. The described local stiffness matrix ***k*** is given as follows:

$$k = \begin{bmatrix} \frac{EA}{L} & 0 & 0 & -\frac{EA}{L} & 0 & 0 \\ 0 & \frac{12EI}{L^3} & \frac{6EI}{L^2} & 0 & \frac{-12EI}{L^3} & \frac{6EI}{L^2} \\ 0 & \frac{6EI}{L^2} & \frac{4EI}{L} & 0 & \frac{-6EI}{L^2} & \frac{2EI}{L} \\ \frac{-EA}{L} & 0 & 0 & \frac{EA}{L} & 0 & 0 \\ 0 & \frac{-12EI}{L^3} & \frac{-6EI}{L^2} & 0 & \frac{12EI}{L^3} & \frac{-6EI}{L^2} \\ 0 & \frac{6EI}{L^2} & \frac{2EI}{L} & 0 & \frac{-6EI}{L^2} & \frac{4EI}{L} \end{bmatrix} \quad \textbf{[2.1]}$$

where E is the elastic modulus of the plane frame element, A is the cross-sectional area, I is the second moment of area, L is the length of the element. The matrix is a representation of the local stiffness matrix with respect to the local coordinate system relative to the plane frame axial direction as seen in Figure 2.2 above. The computation of the local stiffness matrix is followed by its transformation to the global stiffness matrix as given by the formula below:

$$K = T^T \cdot k \cdot T \quad \textbf{[2.2]}$$

where T is the transformation matrix as given below:

$$[T] = \begin{bmatrix} \cos\theta & \sin\theta & 0 & 0 & 0 & 0 \\ -\sin\theta & \cos\theta & 0 & 0 & 0 & 0 \\ 0 & 0 & 1 & 0 & 0 & 0 \\ 0 & 0 & 0 & \cos\theta & \sin\theta & 0 \\ 0 & 0 & 0 & -\sin\theta & \cos\theta & 0 \\ 0 & 0 & 0 & 0 & 0 & 1 \end{bmatrix} \quad \textbf{[2.3]}$$

The resulting global stiffness matrix of the considered plane frame element is then assembled with all other stiffness matrices from other elements to form the system stiffness matrix for the forest. The carbon nanotube forest is then examined in order to compute the distance between nodes. The nodes that fall within a predetermined capture distance of 50nm are assumed to be in contact due to van der Waals force. This predetermined capture distance is measured relative to the outer diameters of all surrounding nodes. The implication being that nodes within the capture distance may reside on two distinct carbon nanotubes or on the same carbon nanotube. After establishment of proximity, an elastic bar

element is introduced between the nodes to simulate the van der Waals force. The introduced bar element is allowed axial and transverse displacement thereby contributing a total of 4 degrees of freedom with 2 degrees of freedom per node. The spring constant of the bar element is given as 273N/m in order to ensure an almost infinitely stiff connection which prevents separation of nodes in contact. The local stiffness matrix of each bar element in the forest is transformed to the global coordinate system and assembled to the system stiffness matrix which now includes both plane frame elements and bar elements.

Furthermore, the proximity of carbon nanotubes in the carbon nanotube array is evaluated by considering the distance between each node in relation to all other nodes in the system. Herein, nodes within a predefined minimum distance are considered to be in contact due to the influence of van der Waals forces. For the current study, the predefined distance is set at 50nm relative to the outer diameters of near neighbor nodes. It must be noted that nodes within the predefined distance could reside on two distinct carbon nanotubes or may even reside on the same carbon nanotube. This scenario allows carbon nanotubes to enter into and retain contact with themselves even under sufficient deformation.

Consider two nodes within the capture distance, a non-physical linear elastic bar element is automatically introduced between the nodes to model the van der Waals force. Herein, the bar element is allowed to possess axial and transverse degrees of freedom per node thereby contributing four degrees of freedom in total. The spring constant of the bar element is established as 273 N/m in order to simulate a nearly infinite stiff connection and ensure a permanent connection between contacting nodes. Like the plane frame elements, the local stiffness matrices of the bar elements are transformed and appropriately added to

the global stiffness matrix thereby completing the assembly of the system global stiffness matrix.

Deflection of the carbon nanotube forest due to the base growth mechanism is subsequently evaluated. Herein, carbon nanotube growth occurs by a two-step process in which the bottom most elements of each carbon nanotube (immediate elements to the substrate) are first extended and then divided to produce a new generation of plane frame elements at the forest substrate. Firstly, each substrate plane frame element is given 100% strain along its growth orientation angle thereby producing an applied tensile force equal to EA at the top-most node of the element. Subsequently, deflection of the carbon nanotube forest is computed based on the application of these forces to the top node of the bottom-most plane frame elements and by solving the given equation below:

$$\{F\}_t - [K]_{t-1}\{U\}_{t-1} = [K]_t\{U\}_t \quad \textbf{[2.4]}$$

where $\{F\}$ is a column vector representing the applied forces, $[K]$ is the global stiffness matrix and $\{U\}$ is a column vector depicting nodal displacements of the system. The subscripts t and t-1 denotes the present and previous time steps respectively. The subtraction of the reaction forces from the previous time steps is representative of the updated Lagrangian method. The substrate anchored nodes represent the point of application of the boundary conditions wherein zero deflection is enforced (x and y directions) and an orientation angle consistent with earlier assigned angles in the nucleation phase. Save for the substrate nodes, all other nodes in the forest are free to translate based on the interactions determined by the global stiffness matrix. Finally, the matrix is solved

for the displacement vector $\{U\}$, which represents the displacement of each node in the system which is due to the growth of the bottom-most series of frame elements.

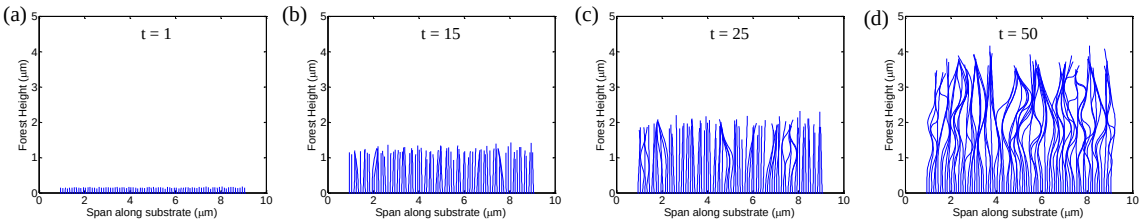

Figure 2.3 Evolution of carbon nanotube growth. (a) Nucleation and normal growth to the substrate, (b) initial contact (c) initial deformation and subsequent growth of carbon nanotube contact, and (d) bending and buckling of forest.

The current deformed state of the forest is obtained by applying the nodal displacements to each node in the system in order to achieve the newly-grown forest. This is closely followed by the division of the elongated plane frame elements at the substrate. The plane frame elements are subdivided in half to create two connected plane frame elements having the same length and orientation angle. Therefore, the bottom most plane frame elements denote the newly-grown carbon nanotube segments, whilst the top-most divided elements represent the carbon nanotube segment identical to the element previously residing at the substrate. This approach ensures that the plane frame elements, nodes and degrees of freedom increase with each new time step. The sequence of carbon nanotube growth is given in figure 2.3 above.

The finite element model is used to carry out a parametric study that considers the growth rate distribution, carbon nanotube diameter, and orientation angle on the resulting forest morphology as presented in Table 2.1. The considered diameters include 5nm, 25nm, and 50nm which is consistent with the diameters of multi-walled carbon nanotubes. The Gaussian distribution is used for the modeling of the growth rates and orientation angles

Table 2.1.1 Parameter variation for study

	Parameter State	Outer Diameter (nm)	Growth Rate Std. Dev.	Angle Std. Dev.
Rate Variation	1	25	5%	5%
	2	25	10%	5%
	3	25	20%	5%
Diameter Variation	1	5	5%	5%
	2	25	5%	5%
	3	50	5%	5%
Angle Variation	1	25	5%	2%
	2	25	5%	5%
	3	25	5%	10%

where the average growth rate is held at 75nm/step and the average orientation angle is 90^0 for all simulation runs. Furthermore, the growth rate standard deviations include 5%, 10% and 20% of the average growth rate, while the orientation angle standard deviations were 2%, 5% and 10% of the stipulated average value. In order, to ensure a consistent parametric study, all the simulations are scaled based upon a single instance in which the growth rate and orientation angles are selected randomly from the normal probability density functions utilizing standard deviations of 20% for the growth rate and 10% for the orientation angle. Subsequent scaling of the growth rate and orientation angle standard deviation in an individual scale is carried out by linearly scaling the difference between the local value and the average value of the scaled parameter using the relationship:

$$X_{new} = C(X_{random} - X_{average}) \text{ [2.5]}$$

where X represents the scaled parameter (growth rate or orientation angle), C represents a scaling factor, and the subscripts “new”, “random” and “average” represent the newly scaled variable, randomly scaled variable from random distribution and the average value of the considered variable (75nm/step for rate and 90° for orientation angle). The approach ensures that only the magnitude of the variation in selected variables change between simulations. This technique supersedes random selection of new distributions for each simulation because it accurately shows the effect of scaling these parameters for the modest population size of the simulations. Similarly, when a given parameter is varied all other parameters are held constant. The default values include 25nm for outer diameter, growth rate standard of 10% of the population average, and an orientation standard deviation of 5% of the population average. The end result is that all the parameter studies share one common set of growth study.

The simulations were run in MATLAB 2013b on a Windows 8 desktop PC with an Intel Core PC with an Intel Core i7-4770 3.4GHz processor and 32GB RAM. The time frame of a typical simulation considering a population of 100 carbon nanotubes grown for 200 time steps is approximately 10.5 minutes. The outputs are graphical plot files depicting the morphology at each time step (*.png and *.emf file formats).

2.3 Results and discussions

The carbon nanotube growth begins with straight-line growth of carbon nanotubes defined by the orientation angles and growth rates defined during the nucleation phase. Subsequent time steps will see the establishment of physical contact between carbon nanotubes that

come within the predefined capture distance as earlier stated. After contact, the van der Waals interaction act to keep this connection. The reaction forces that lead to translation, rotation and bending of carbon nanotubes are generated as a result of the mismatch between the growth rates and orientation angles. It has been noticed that contacting carbon nanotubes with large mismatches in growth rate will translate, rotate and eventually buckle in response to the reaction forces. With subsequent growth, these interactions become increasingly complex and the forest becomes highly convoluted and interconnected. A time-resolved evolution of a typical carbon nanotube population is seen in Figure 2.3 where the nucleation to the formation of an interconnected forest is clearly delineated. The results of the parametric study after 200 time steps are shown in Figure 2.4 below.

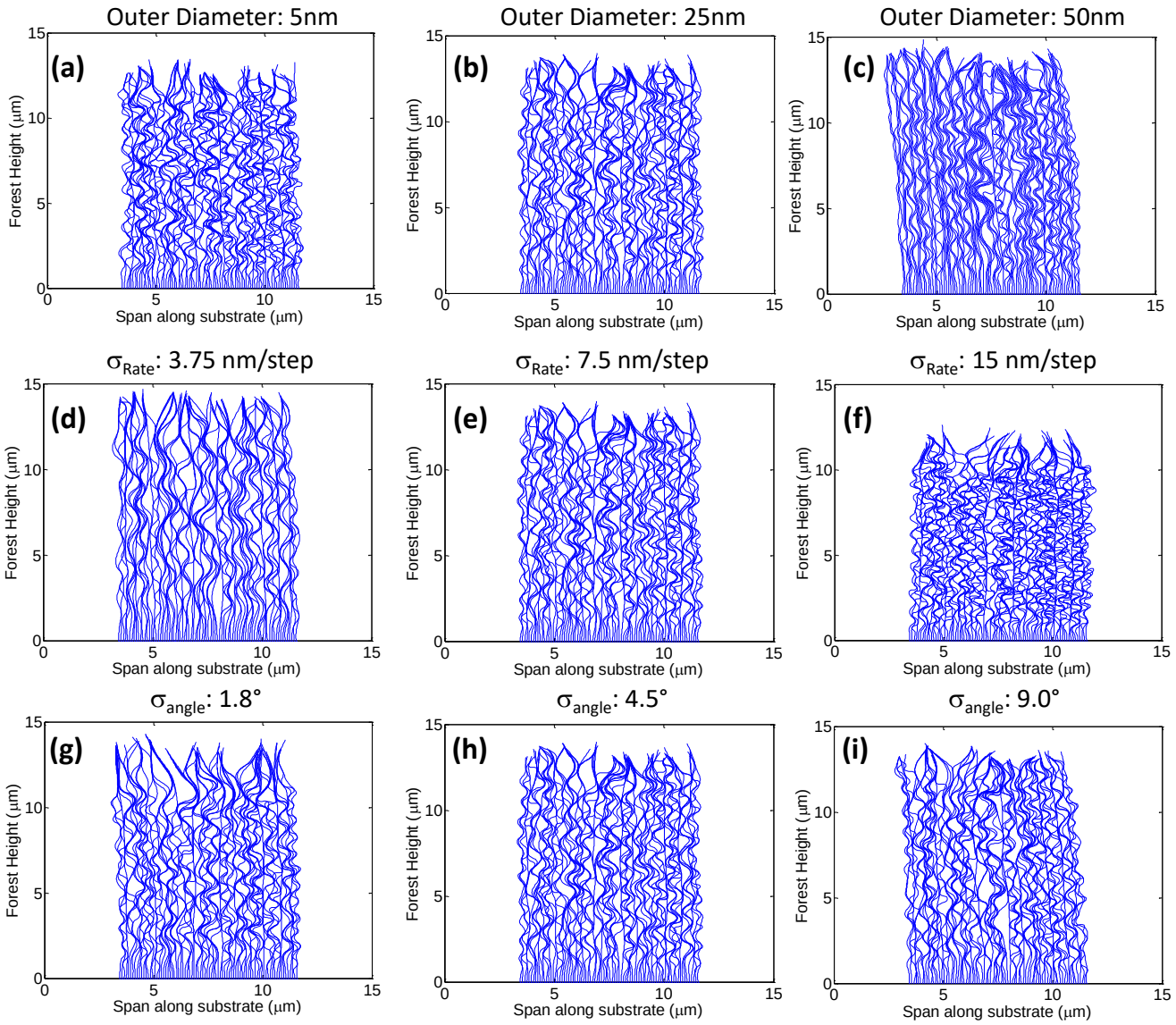

Figure 2.4 Forest morphologies emanating from parametric study of (a-c) diameter, (d-f) growth rate distribution, and (g-i) orientation angle distribution. For all studies, all parameters are held constant whilst the varied parameter is held constant. The variation of parameters leads to a single case of homogeneity in terms of morphology as seen in (b, e, h).

Further analysis of the forest is carried out using the Herman Orientation Factor (HOF).

Herein, the HOF is computed by analyzing the 2-D Fast Fourier Transform (FFT) intensity of a carbon nanotube morphology image using the expressions found below:

$$HOF \equiv \frac{1}{2}(3\langle \cos^2 \varphi \rangle - 1) \quad \textbf{[2.6]}$$

$$\left\langle \cos^2 \varphi \right\rangle = \frac{\int_0^{\frac{\pi}{2}} I(\varphi) \cos^2 \varphi \sin \varphi d\varphi}{\int_0^{\frac{\pi}{2}} I(\varphi) \sin \varphi d\varphi} \quad \textbf{[2.7]}$$

where the angle φ is measured relative to the greatest intensity of the analyzed image. Perfect alignment is denoted by an HOF value of 1 while lesser values represent reduced alignment along a preferred axis. In this study, a 5 x 5μm section is cropped from the middle of each carbon nanotube forest and analyzed by 2-D FFT. For further analysis, the FFT intensity map was analyzed using equations 2.6 - 2.7 in order to get the depictive HOF for each forest. The resulting HOF values are seen in figure 2.5 where they have been computed using the finite FFT spectra.

2.3.1 Effect of Diameter Variation

Bending stiffness of the carbon nanotubes is a function of the inner and outer radius of the tubes. In specific terms, the modulus of each carbon nanotube is constant, while the bending stiffness, EI, is a function of only the second moment of inertia, I.

$$I = \frac{\pi(r_o^{\,4} - r_i^{\,4})}{2} \quad \textbf{[2.8]}$$

where r_o and r_i are the outer and inner radii of the carbon nanotube respectively. The consequence being that small diameter carbon nanotubes possess less resistance to bending during interactions with neighboring carbon nanotubes. The result is that small diameter carbon nanotubes can significantly accommodate greater curvature than larger diameter carbon nanotubes in response to the reaction forces generated within a growing carbon nanotube forest. The morphological differences emanating from the variation of carbon

nanotube diameter is seen if figure 2.4(a-c). Note that the angular orientation distribution and growth rate standard deviation are identical in this case. In each forest simulation, highly convoluted carbon nanotubes are seen to mix among the carbon nanotubes that remain nearly vertical and straight from the free ends of the forest to the nucleation substrate, particularly for outer diameters of 5nm and 25nm. It is significant to note that the curvature of tortuous carbon nanotubes decreases as diameter increases due to increase in the bending stiffness. In addition, the carbon nanotube forest height increases from a height of 13.5μm to 14.9μm when increasing the carbon nanotube diameter from 5nm to 50nm as a result of the less tortuous growth path. As seen in figure 2.5, the HOF increases from 0.19 for a forest with 5nm diameter carbon nanotubes to 0.43 for a forest with 50nm diameter carbon nanotubes, therefore indicating an increase in carbon nanotube alignment within the forest. Finally, the spacing between the outer diameters of carbon nanotubes is significantly increased from 5nm to 50nm, albeit the pitch between forest carbon nanotubes is constant at 100nm. This observation is consistent with previously reported data [50].

2.3.2 Effect of Growth Rate Variability

It has been shown experimentally that the growth rate of carbon nanotubes vary significantly as a function of precursor gas, catalyst diameter and growth time. Herein, these relationship is modeled using the Gaussian distribution of carbon nanotube growth rates whereby an increase in growth rate standard deviation within the forest leads to a corresponding increase in the growth rate of the fastest growing carbon nanotube and a decrease in the growth rate of the slowest growing carbon nanotube. On a whole, the average growth rate is held constant for these simulations. When nanotubes with distinct growth rates contact, the faster growing carbon nanotube is significantly hindered by the

slower growing carbon nanotube and this leads to bending or buckling in the faster growing carbon nanotube. As tortuosity and interconnectivity increases in the forest, the influence of the slowly growing carbon nanotube permeates thereby limiting the attaining of higher heights by the forest.

From the results, it is seen that the tortuosity of simulated forests increases significantly as the growth rates increases from 5% to 20% of the average population mean as seen in Figure2.4(d-f). The forest height is noticed to decrease from 14.7μm at a growth rate standard deviation of 5% to 12.6μm at a standard deviation of 20%. In spite of half of the carbon nanotubes growing at a faster rate due to standard deviation increase, a decrease in forest height occurs notwithstanding. This portends that height advancement in carbon nanotube forests is directly influenced by the growth rates of the slow carbon nanotubes. The considerable value of van der Waals stiffness imposed for contacting nanotubes discourage the breaking of the van der Waals bonds that could occur in a real forest.

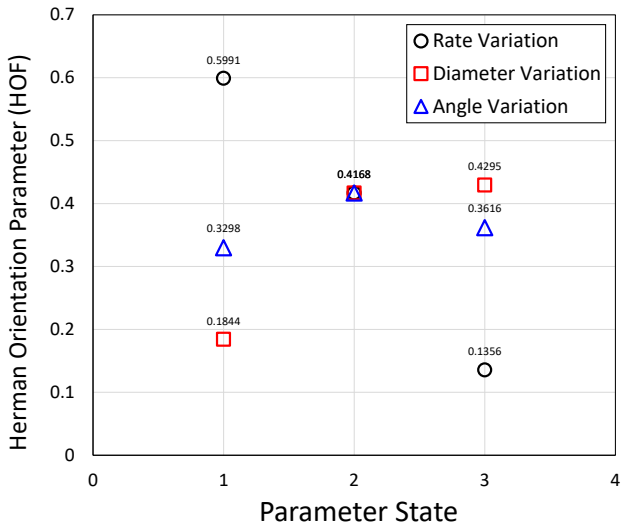

Figure 2.5 Herman's Orientation Factor for each of the morphology in the parametric study. The parameters include rate variation, diameter variation, and orientation angle variation as shown in Table 2.1 above.

The loss of vertical alignment or increased tortuosity emanating from increased growth rate standard deviation is evidenced by a decreasing HOF as seen in figure 2.5. Herein, the HOF decreases from approximately 0.6 at a standard deviation of 5% to approximately 0.14 for the forest grown with a 20% standard deviation. This effect is the most vivid of all observed effects from our parametric study.

2.3.3 Effect of Orientation Angle Variability

The orientation angle is modeled as a normal distribution which is normal to the growth substrate. Not considering carbon nanotube mass and thermal vibrations, the orientation angle variability is the single most parameter responsible for contact and interaction of neighboring carbon nanotubes. Take for example, a reduced orientation angle standard deviations will require that carbon nanotubes acquire a greater length before coming to contact with a neighboring carbon nanotube as opposed to a forest with a greater orientation angle standard deviation. At contact, the mismatch between growth rates dominates the interactions that determine the carbon nanotube forest morphology. This is evident in figure 2.4(g-i) which shows a similar morphology between all forests except for areas near the top surface of the forests. For the 2% orientation angle standard deviation, less connectivity is seen at the top surface whilst maintaining a near vertical orientation. For forests grown at a 5% and 10% orientation angle standard deviation, there is an increase in uniform interconnectivity and tortuosity from the top to the bottom of the forest. Save for the forest top, the forest morphologies are quite similar thereby hinting that the forest morphology is relatively insensitive to the orientation angle distribution of the constituent carbon nanotubes. This pattern is obvious in figure 2.5 where the HOF between the carbon nanotube forests relatively insensitive to changes in the standard deviation.

This parametric study proves that variations in carbon nanotube forest morphology could be achieved by employing the carbon nanotube forest growth model. Furthermore, just like experimental grown forests the simulated forest morphology could also be analyzed after growth. Although, a simplified distribution of forest parameters was utilized to proof the functionality of the model, a distribution more consistent with experimentally observed values could be applied. Also, modifications could be made to factor in the complex van der Waals potential in order to account for its diameter dependence and carbon nanotube radial deformation induced by contact forces. Parameters like finite catalyst lifetime and time-dependent growth rates can also be introduced in order to incorporate temporal component. This will likely introduce the height-dependent morphological gradients that are prevalent in tall carbon nanotube forests.

2.4 Conclusions

A finite element model of actively growing carbon nanotubes is employed to conduct a parametric study which investigates variable carbon nanotube diameter, growth rate distributions and orientation angle distributions. The resultant model morphology shows strong consistency with experimental results and exhibit similar trends as expected. For simplification purposes, the model is left simple to demonstrate functionality and viability for carbon nanotube modeling. The model is sufficiently suitable for incorporation of more realistic parameter distributions, time-dependent parameters, and more geometrically complex substrates (such as radial geometries) can be appropriately integrated if they are experimentally known.

Finally, the model could be subjected to mechanical, thermal and electrical evaluation after growth thereby ensuring that a carbon nanotube forest maybe modeled from synthesis

to application. A model with the aforementioned capability will ensure holistic control and understanding of the intricate complex interactions in a forest and allow for a knowledgeable selection of growth parameters to improve the functionality of a given application.

Chapter 3 Simulating the Axial Force at the Substrate of a Growing Carbon Nanotube Forests

3.1 Introduction

The morphology of a carbon nanotube forest is known to play a significant role in the performance metrics of forests. In spite of its significant role, the complex interactions that help influence the forest morphology during synthesis have not been well understood. A comprehensive understanding of the inherent interactions amongst carbon nanotubes is necessary for understanding, predicting and control of the forest morphology for desired applications.

Chemical vapor deposition is the most widely employed approach for the synthesis of carbon nanotube forests. Herein, hydrocarbons are pyrolyzed in the presence of metal films or particles that serve as catalysts. The synthesis/growth method of carbon nanotubes can be classified into either the tip growth or the base growth methods. In the tip growth method, catalyst particles reside at the tip of a growing tube as opposed to the base growth approach where catalyst particles reside at the growth substrate for the duration of growth.

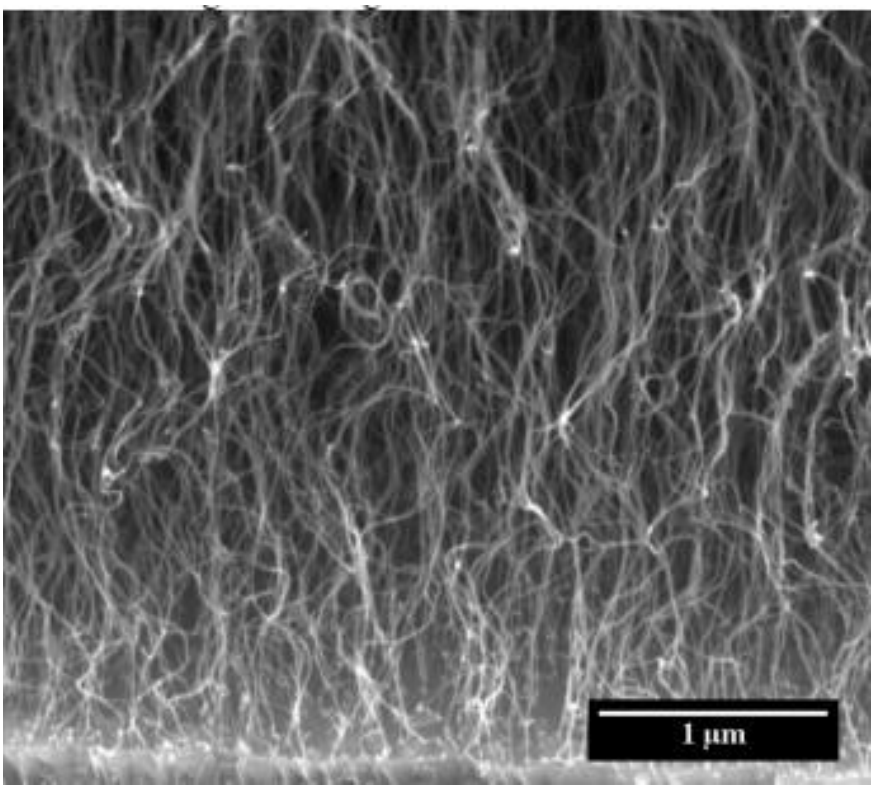

Figure 3.1 SEM micrograph of a convoluted carbon nanotube forest.

The formation of carbon nanotube forests occurs when a dense population of nanotubes are grown in tandem whilst maintaining a close proximity. The vertical orientation of carbon nanotubes in a forest are as a result of the crowding forces that arise due to close proximity while the tortuous paths are predetermined by individual tubes. Due to the existent mismatch in population growth rates, the normal force applied to the substrate catalyst is expected to be non-uniform and may influence the rate of catalytic activity. This suggests that an increased loading may result in the delamination of carbon nanotubes therefore disrupting overall forest growth.

Herein, a 2-dimensional finite element model of a growing carbon nanotube forest is developed with considerations given to the carbon nanotube growth rate, outer diameter, inner diameter, growth orientation angle, and elastic modulus. A time-resolved evolution

of carbon nanotube forest is achieved by assembling linear elastic plane frame elements at specific time steps and modeling of van der Waals force by the use of linear elastic bar elements. The bar element is introduced when carbon nanotube nodes come within a predetermined capture distance after which contact is said to be established between the considered nodes. For subsequent time steps, the carbon nanotubes remain in contact unless forces arise and break the contact.

3.2 Modeling Procedure

Carbon nanotube modeling begins by nucleation at the substrate where the inner diameter, outer diameter, growth rate, and orientation angle are appropriately assigned. The procedure is akin to the earlier described steps (chapter 2) where subsequent growth steps also maintain the nucleation assigned parameters. In this study, a forest of 100 uniformly spaced carbon nanotubes is grown on a 15μm substrate for 250 time steps. The resulting forest has an equivalent linear density of 6.7 tubes/μm on a 3-D substrate. The employed growth rates and orientation angle distribution are based on a Gaussian probability density function. For the growth rate distribution, an average of 50nm/step is inputted while the orientation angle is given an average of $\pi/2$ (in other words normal to the substrate). For the study, the growth rates are varied using standard deviations of 2%, 10% and 20% whilst maintaining a constant angular orientation of 10% in order to ensure accuracy in the comparison.

As earlier stated, the nucleation phase entails assignment of carbon nanotube properties and location which remain for the duration of the growth sequence. The plane frame element is modeled at each pre-assigned nucleation site which is then followed by the computation of the forest stiffness matrix that accounts for the stiffness matrices of

individual carbon nanotubes in the model. Below is the stiffness matrix of a single plane frame element in the local coordinate system which will be transformed to the global coordinate system. In the matrix shown, E is the elastic modulus, I is the second moment of inertia, A is the tubular cross sectional area and L is the length of the plane frame elements. The assemblage of the forest stiffness matrix is followed by the evaluation of the distance between adjacent carbon nanotubes nodes after which the bar element is introduced for nodes that come within the predefined capture distance therefore modeling van der Waals force between nodes. This is followed by the transformation of the utilized bar element to the global coordinate system after which it is appropriately added to the forest stiffness matrix thereby completing the assemblage of the forest stiffness matrix.

$$k = \begin{bmatrix} \frac{EA}{L} & 0 & 0 & -\frac{EA}{L} & 0 & 0 \\ 0 & \frac{12EI}{L^3} & \frac{6EI}{L^2} & 0 & \frac{-12EI}{L^3} & \frac{6EI}{L^2} \\ 0 & \frac{6EI}{L^2} & \frac{4EI}{L} & 0 & \frac{-6EI}{L^2} & \frac{2EI}{L} \\ \frac{-EA}{L} & 0 & 0 & \frac{EA}{L} & 0 & 0 \\ 0 & \frac{-12EI}{L^3} & \frac{-6EI}{L^2} & 0 & \frac{12EI}{L^3} & \frac{-6EI}{L^2} \\ 0 & \frac{6EI}{L^2} & \frac{2EI}{L} & 0 & \frac{-6EI}{L^2} & \frac{4EI}{L} \end{bmatrix} \quad \textbf{[3.1]}$$

The deflection of the substrate bound nanotubes due to the base growth mechanism is subdivided into two steps: (i) stretching of carbon nanotubes along the assigned orientation angle, (ii) division of stretched plane frame elements in order to form a new set of carbon

nanotubes. The deflection of the plane frame elements is evaluated using an updated Lagrangian modeling approach

$$\{F\}_t - [K]_{t-1}\{U\}_{t-1} = [K]_t\{U\}_t \quad \textbf{[3.2]}$$

where $\{F\}_t$ is a column vector of applied forces, $[K]_t$ is the forest stiffness matrix which defines both the rigidity of each carbon nanotube and the van der Waals force in the forest. The model generated plots of carbon nanotube populations show strong similarities with experimentally grown forests. For instance, the tortuosity and bundling of carbon nanotubes is clearly seen in the model representations of carbon nanotube forests. Figure 3.2 shows the evolution of carbon nanotube growth from nucleation to growth termination for 250 time steps.

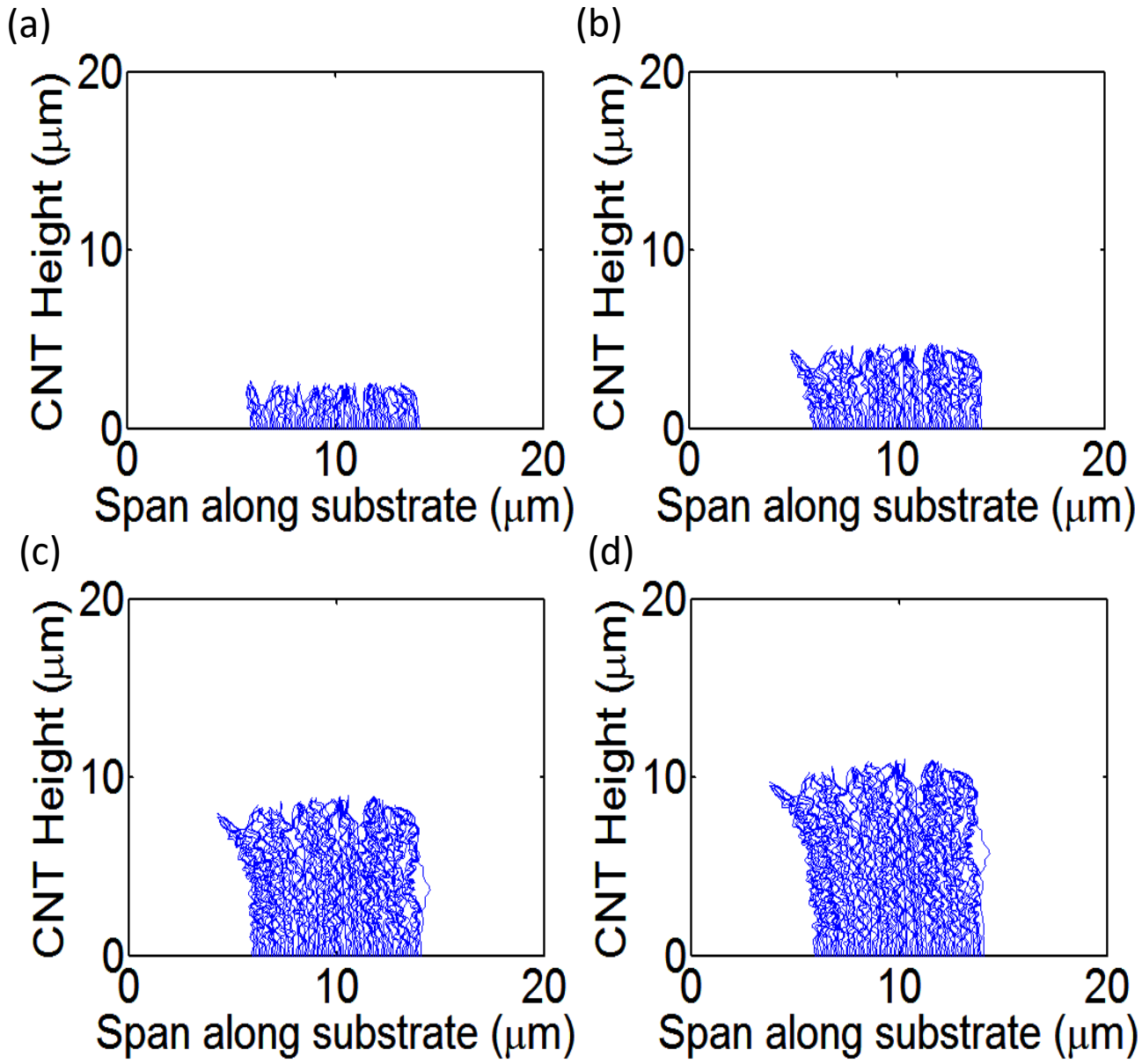

Figure 3.2 Evolution of CNT growth for 250 time steps. (a) 50 growth steps, (b) 100 growth steps, (d) 200 growth steps, (e) 200 growth steps, (f) 250 growth steps.

A parametric study was carried out on the finite element model to determine the effects of varying the growth rate on the axial forces generated at the catalyst particle residing at the substrate of the forest. The desired goal is to better understand the effects of axial forces on the catalyst located at the substrate of the forest. The growth rate distributions were varied using standard deviations of 2%, 10%, and 20% whilst keeping all other parameters

constant. The parameters assigned to individual carbon nanotubes include inner diameter of 7nm, outer diameter of 10nm and elastic modulus of 1TPa. The carbon nanotube forest was grown on a substrate with uniform spacing amongst neighboring nanotubes. For the orientation angle of carbon nanotubes, each carbon nanotube was assigned values based on one instance of random selection of an angular standard deviation of 10% from the substrate normal. This randomized initial distribution is now employed for subsequent simulations to ensure consistency and accuracy in the study. The growth rate of the carbon nanotube forest is assigned based on an average growth rate of 50nm per time step and a standard deviation of 10nm per time step. The randomization of the growth rate distribution is followed by its scaling linearly relative to the assigned average growth rate. This ensures that the growth rate between each simulation is scaled relative to one another as opposed to random reassignment for each simulation. This approach ensures that the growth rate mismatch between neighboring carbon nanotubes (contacting carbon nanotubes) will scale with the variation in standard deviation.

Herein, the axial forces are evaluated with respect to the local coordinate system of each element. Also, the element coordinates are examined with respect to the longitudinal axis of the carbon nanotubes. Axial force representation in the local coordinate system allows for an easy interpretation of the stress state present in each element. Special consideration is given to elements located at the growth substrate since they are responsible for force transmission to the catalyst particle and substrate.

3.3 Results and Discussion

The fastest and slowest growing carbon nanotubes in the forest population are identified during nucleation and then subsequently chronicled for the following time steps. The

emphasis is on the forces transmitted to the catalyst particle. Force acting on the catalyst particle may be sufficient to introduce defects, alter growth rate, translate the particle, or even cease growth altogether. To perform this analysis, the axial forces generated at the second elements from the substrate are interrogated. This approach is taken because the bottom-most element is artificially stretched and divided during the growth process and hence do not provide accurate representation of the forces transmitted to the catalyst particle. The forces in the second set of elements from the substrate are accurate depiction of the reaction forces resulting from the growing carbon nanotube forest. Due to the transmission of load between the second elements and the bottom elements, the force in the second elements becomes an accurate representation of the forces experienced by the catalyst particle. Therefore, the axial force at the second layer of elements is recorded for each time step as the forces experienced at the growth substrate. In the forest population, it is reasonable to anticipate that the slowest growing carbon nanotubes in the population will experience a pulling or tension force once contact is established as a result of the influence of van der Waals force.

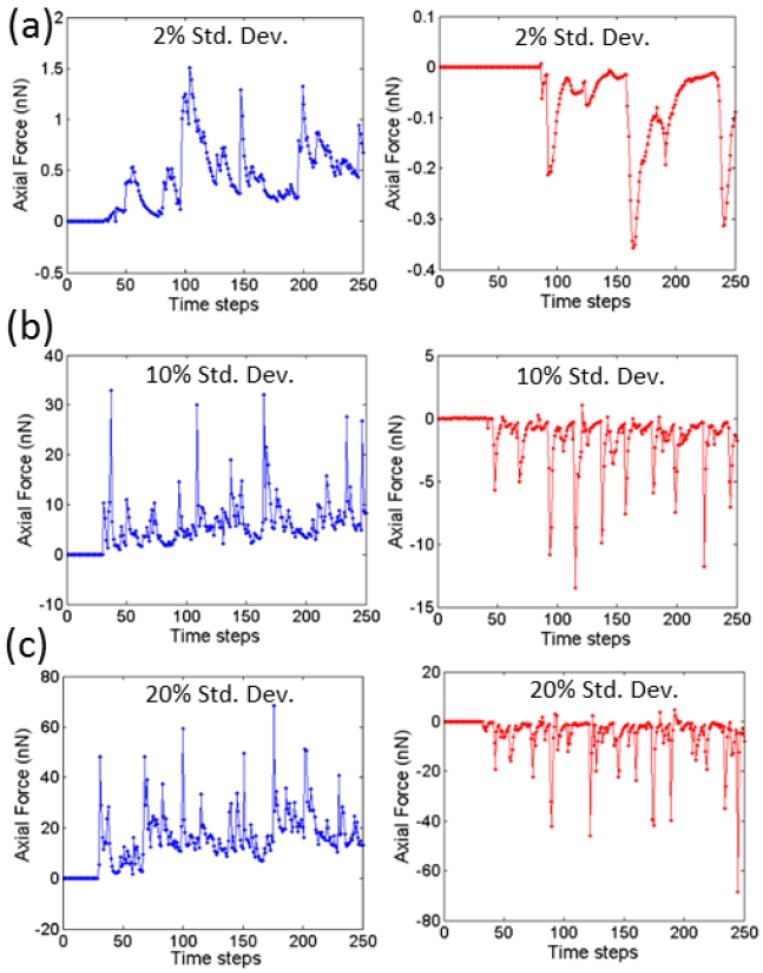

Figure 3.3 Axial Force at the substrate of the slowest (blue) and fastest (red) growing carbon nanotube in forests with varying population standard deviations of (a) 2%, (b) 10%, and (c) 20% of the average growth rate of 50nm per time step.

In contrast, the fastest growing carbon nanotube will experience some sort of drag or compressive force from the population of comparatively slower nanotubes. Due to the high aspect ratio and hollow cores of nanotubes, they offer little resistance to bending. The consequence of this is that carbon nanotubes growing at a rate that supersedes nearest neighbors will fail due to buckling and experience bending moment in addition to the compressive forces of the slower growing carbon nanotubes. Figure 3.3 chronicles the time history of axial force experienced at the substrate of the fastest and slowest growing carbon nanotubes which were grown at 2%, 10% and 20% standard deviations in relation to the average rate of 50nm/step. As earlier predicted, the slowest growing carbon nanotube is in a state of tension after contact as evidenced by the positive axial forces. The fastest growing carbon nanotube in the population, conversely

experiences a compressive force. Once contact is established, a net axial force arises largely due to a mismatch in the growth rate and orientation angles. The magnitude of these values strongly varies as a function of time.

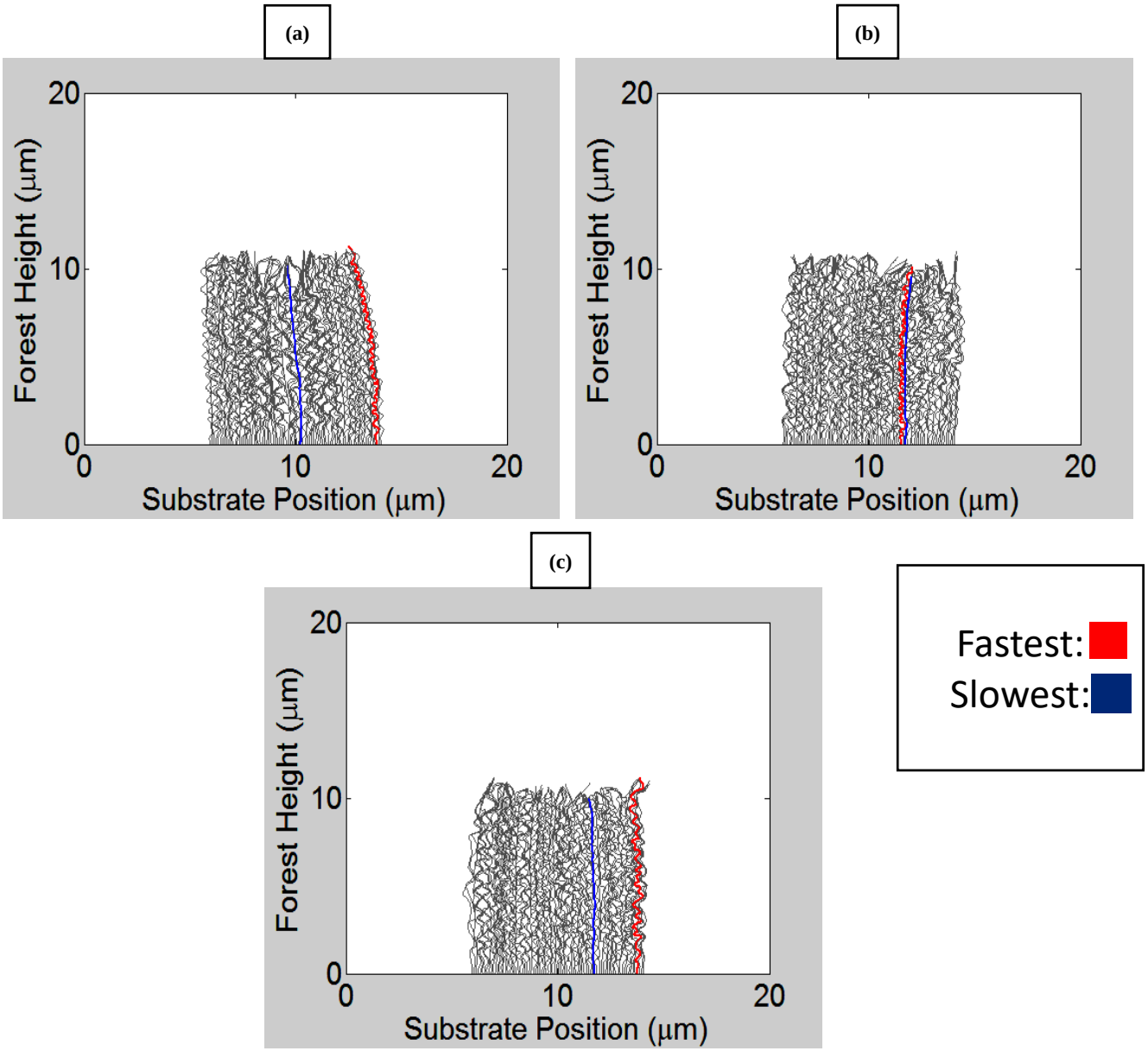

Figure 3.4 Carbon nanotube forests showing the slowest and fastest tubes for: (a) rate standard deviation of 2% (b) rate standard deviation of 10% (c) rate standard deviation of 20%

A peak in the tensile force is seen when the slowest growing carbon nanotube makes contact with neighboring tubes which grow at a comparatively faster rate. This tensile force then decays as the contacting carbon nanotubes deform and share loading with other neighboring tubes. Along the same line, the magnitude of compressive forces as seen in the fastest growing carbon nanotube peaks when new contacts are established near the growth substrate. This is subsequently followed by decay in magnitude as time proceeds. It must be noted that at a relaxed state, the fastest growing carbon nanotube exhibits a nearly neutral axial load as opposed to the slowest growing carbon nanotube which is in a state of perpetual tension after contact is established with neighbors. The slowest growing carbon nanotube will be constantly pulled upward especially in a straight direction hence a constant net tensile force will be perpetually seen. From the plots shown in figure 3.3, the magnitude of forces experienced at the substrate varies strongly as a function of the growth rate variation. This trend is due to an increased mismatch in growth rates between the contacting carbon nanotubes. Recall that all other parameters (including orientation angle) in the model are kept constant during variation in growth rates thereby ensuring that the variation in forces as seen in the plots is strictly due to the mismatch in growth rate. The resultant maximum axial tensile force in terms of pressure varies from approximately 37MPa at 2% standard deviation, 849MPa at 10% standard deviation, to 1772MPaat 20% standard deviation relative to the average growth rate. On the other hand, the maximum compressive load in terms of pressure for the fastest growing carbon nanotube ranges from 87MPa at 2% standard deviation to 350MPaat 10% standard deviation, and 1698Mpa at 20% standard deviation. The peak tensile loads experienced by the slowest growing carbon nanotube is generally greater than the magnitude of compressive loads experienced by the

fastest growing carbon nanotube in a given population. It must be noted that occasionally, the fastest growing carbon nanotube may experience axial tension force at the substrate, while the slowest growing carbon nanotube is under constant tension at the substrate after contacting with neighboring carbon nanotubes. The morphologies of the forests are presented in Figure 3.4.

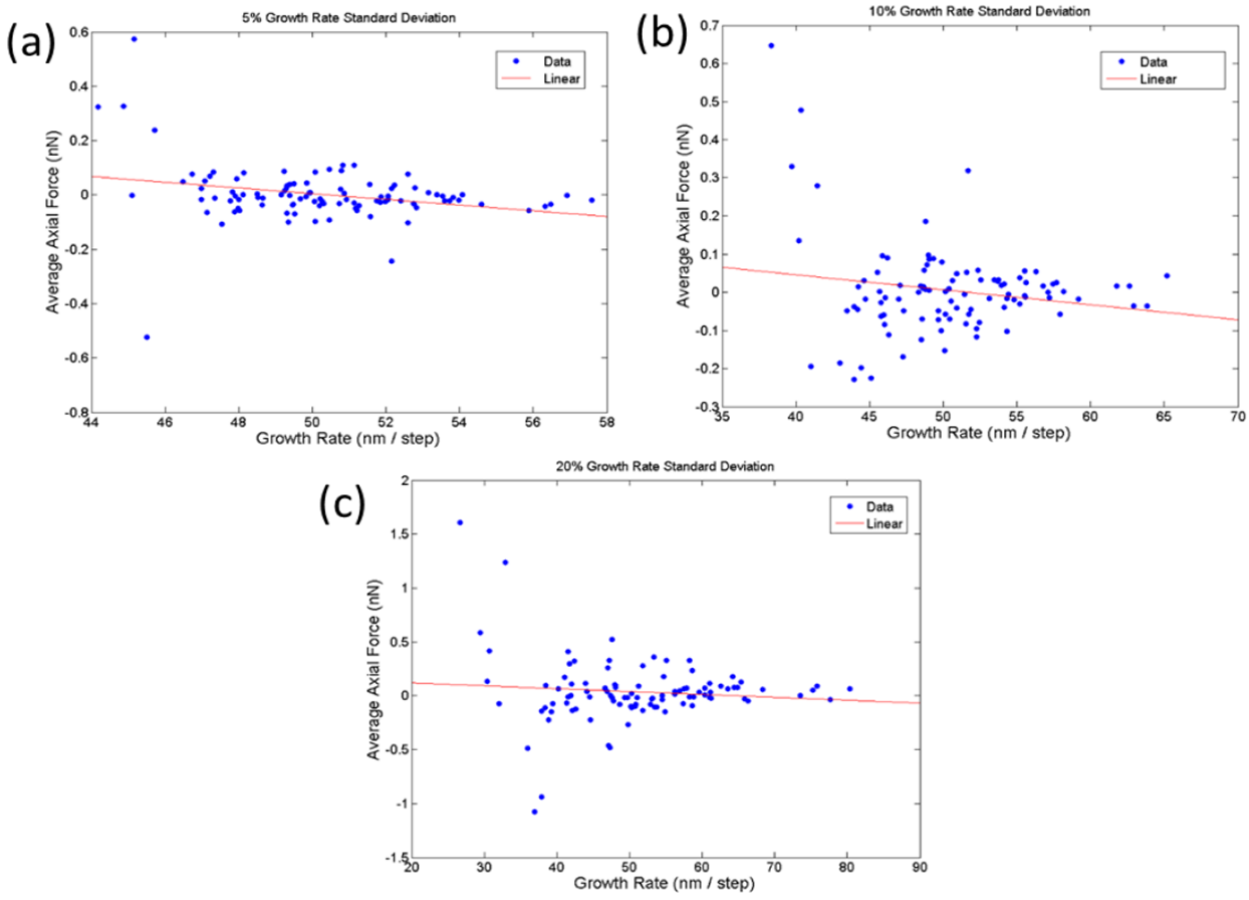

Figure 3.5 Time averaged axial force per carbon nanotube as a function of its growth rate. The above results are plotted for forests having growth rate standard deviations of (a) 2%, (b) 10%, and (c) 20% of the average growth rate of 50nm/time step.

Also, the time averaged axial force is examined at the substrate of the forest population for the last 150 growth steps. The resulting plots are seen in figure 3.5 where the average force is plotted as a function of the carbon nanotube growth rate. The resulting trend shows that the slowest growing carbon nanotube exhibits a time-averaged force that is in tension as

shown by the positive axial forces. The trend in the plot shows a general decrease in axial load as a function of increasing growth rate. However, the nature of the data is generally nonlinear. The slowest growing carbon nanotube was consistently in tension whilst other nanotubes that grow at a rate considerably lower than the population average of 50nm/step exhibit a time-averaged force that was generally compressive in nature. This trend that seems inconsistent is thought to arise due to the random nature of the assigned growth rates. This is because the origin of axial force is believed to be related to the growth rate mismatch between contacting carbon nanotubes. Therefore, the absolute growth rate of a particular carbon nanotube might not be significant when compared to the relative differences in growth rates between a given carbon nanotube and its adjacent neighbors. Also, since a given carbon nanotube may establish contact with multiple neighbors, the force experienced at the substrate of a given carbon nanotube may be a combination of numerous interactions between multiple tubes. Finally, the axial forces at the substrate of most carbon nanotubes are largely neutral in a time-averaged sense with the fastest growing carbon nanotube being no exception.

3.4 Conclusion

An actively growing carbon nanotube forest is modeled using a 2-dimensional finite element modeling approach. The axial force at the forest substrate is analyzed to better understand the mechanical loading as experienced by catalysts during the base growth of carbon nanotubes. The results show that the slowest growing carbon nanotube in the population is perpetually in tension after establishing contact with neighboring carbon nanotubes while the fastest growing carbon nanotube is in compression after making contact with the adjacent slower growing carbon nanotubes. However, this axial

compressive force as seen in the fastest growing carbon nanotube rapidly decays to a nearly neutral loading state. The above results can potentially be employed in examining the load at the substrate of growing carbon nanotube forests with the aim of predicting delamination.

Chapter 4 CNT Forest Population Growth Kinetics

4.1 Introduction

The superlative properties of carbon nanotubes have been lauded from its time of discovery [16] in 1991 to this very day. These exceptional properties include high tensile strength, tremendous electrical properties, thermal properties, optical properties, kinetic properties have inspired potential applications in thermal interface materials [51], in nano-precision actuators [52],in drug delivery [53], in nanosensors [54], in nanocomposites [5] and in electrical interconnects [55]. Notwithstanding these promising properties exhibited by individual carbon nanotubes, it is well documented that the prevalent tortuosity and coupling seen in carbon nanotube forests limits the quality and density of [44] of carbon nanotubes thereby adversely affecting performance in fabricated devices. The complex morphology as seen in carbon nanotube forests arises from the mechanical interactions between growing and interacting carbon nanotubes during collective growth. While the relationship between carbon nanotube forest morphology and mechanical performance have long been established qualitatively, the quantitative structure-property relationship [56] significantly lacks in the literature largely due to the associated complexity in the experimental characterization of the highly anisotropic morphology of carbon nanotube forests. The fundamental need for a complete understanding of the quantitative structure-property relationship of a carbon nanotube forest and the associated difficulty involved in the experimental characterization of carbon nanotubes motivates the choice of a numerical approach for the elucidation of this important problem.

Previous research inputs in this area have employed a somewhat simplification of the physics of carbon nanotube growth whilst modeling carbon nanotube forests as an isotropic

continuum [43], array of interacting beam segments [44], distinct cells of vertically oriented beams [45, 57] and individually oriented vertical beams [41, 42]. These modeling approaches albeit sufficient for their intended problems, they do not capture the complex mechanics of carbon nanotube growth. Herein, a modeling approach that incorporates intra carbon nanotube interaction is presented whilst allowing for the input of varied forest parameters. These forest parameters include carbon nanotube growth rate, angle of inclination, carbon nanotube diameter, span of forest substrate, and number of forest tubes. The stated parameters could be appropriately varied in our model for implementation of various carbon nanotube studies. The modeling approach employed herein allows for a comprehensive study of a growing nanotube forest. The mechanics of two growing and interacting nanotubes is first examined where all associated interactions as seen in a fully grown forest is also prevalent. This is then followed by the study of a 3-D carbon nanotube forest of 1600 tubes in which parameters like growth rate, diameter, and angle of orientation are appropriately predefined.

The numerical model of the forest employs the finite element method where carbon nanotubes are modeled as plane frame elements and associated van der Waals forces between carbon nanotubes are modeled using bar elements. The properties of individual carbon nanotubes like diameter, elastic modulus, cross-sectional area, moment of inertia and spatial density of the forest are all predefined before the growth sequence. The finite element model assumes linearity of all interactions in the forest whilst ensuring a fixed boundary condition at the substrate of the forest. The evaluation of the forest deformation involves the solving of large matrices as it pertains to individual nanotubes where the essential boundary conditions at the substrate significantly reduces the size of the

assembled matrix we are required to solve. The solution of displacement from the array stiffness matrix and stretching force signifies the end of a given growth step. Subsequent growth steps will factor in the previous displacement.

4.2 Experimental Details

The carbon nanotube model employed is aligned with the chemical vapor deposition method of synthesizing nanotube forests. In brief, carbon nanotubes are modeled as growing from anchored catalyst particles affixed to a rigid substrate by the base growth mechanism. This model allows for a choice of the number of nucleated carbon nanotubes, their respective diameters, growth rates, growth orientation angle and the magnitude of van der Waals force between interacting carbon nanotubes. Herein, carbon nanotubes are modeled as 2-dimensional and 3-dimensional frame elements (Figures 2.2 and 4.1 respectively) which allow for the capture of the linear elastic deformation phenomenon as seen in a fully grown forest. The 3-dimensional frame element allows 6 degrees of freedom per node which cumulates to 12 degrees of freedom per element. Figure 4.1 below explicitly shows the degrees of freedom of a 3-D frame element where q_1, q_2, q_3 are the

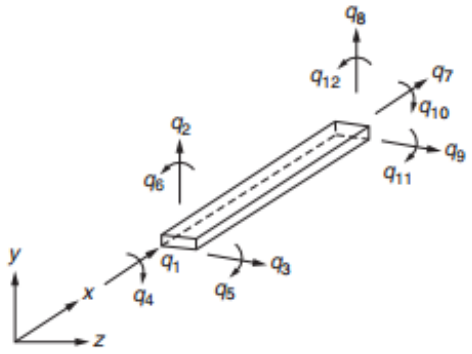

Figure 4.1 Schematic diagram showing a 3-dimensional frame element employed in the modeling of a typical carbon nanotube with the corresponding degrees of freedom shown [58].

displacements at node 1 while q_4, q_5 and q_6 are the corresponding rotations. The growth sequence begins with the nucleation of carbon nanotubes at the substrate where the user defined properties are assigned to each nanotube. The initial growth step is characterized by the normal orientation of carbon nanotubes with respect to the substrate where the much expected interactions between nanotubes are absent. At this point, a global stiffness matrix of all carbon nanotubes in the forest is assembled where each stiffness matrix per carbon nanotube is appropriately added in accordance with its degrees of freedom. This addition to the global stiffness matrix is preceded by the transformation of the local stiffness matrix of each carbon nanotube from the local coordinate system to the global coordinate system. Furthermore, the global stiffness matrix of all bar elements employed in the modeling of van der Waals force is also assembled to the global stiffness matrix. The assembled bar elements are linear elastic elements with a cumulative 4 degrees of freedom in which 2 degrees of freedom are imposed per node. The degrees of freedom for the bar element correspond to axial and transverse displacements. They are introduced between carbon nanotubes which are in close proximity and which fall within a predefined capture distance. The magnitude of van der Waals force between contacting carbon nanotubes and the capture distance play a vital role in determining the resulting morphology of the forest. Assembly of the global stiffness matrix is followed by the evaluation of the displacement of the carbon nanotubes using the static equilibrium equation in [3.2] where the applied forces are in the longitudinal direction of the carbon nanotubes.

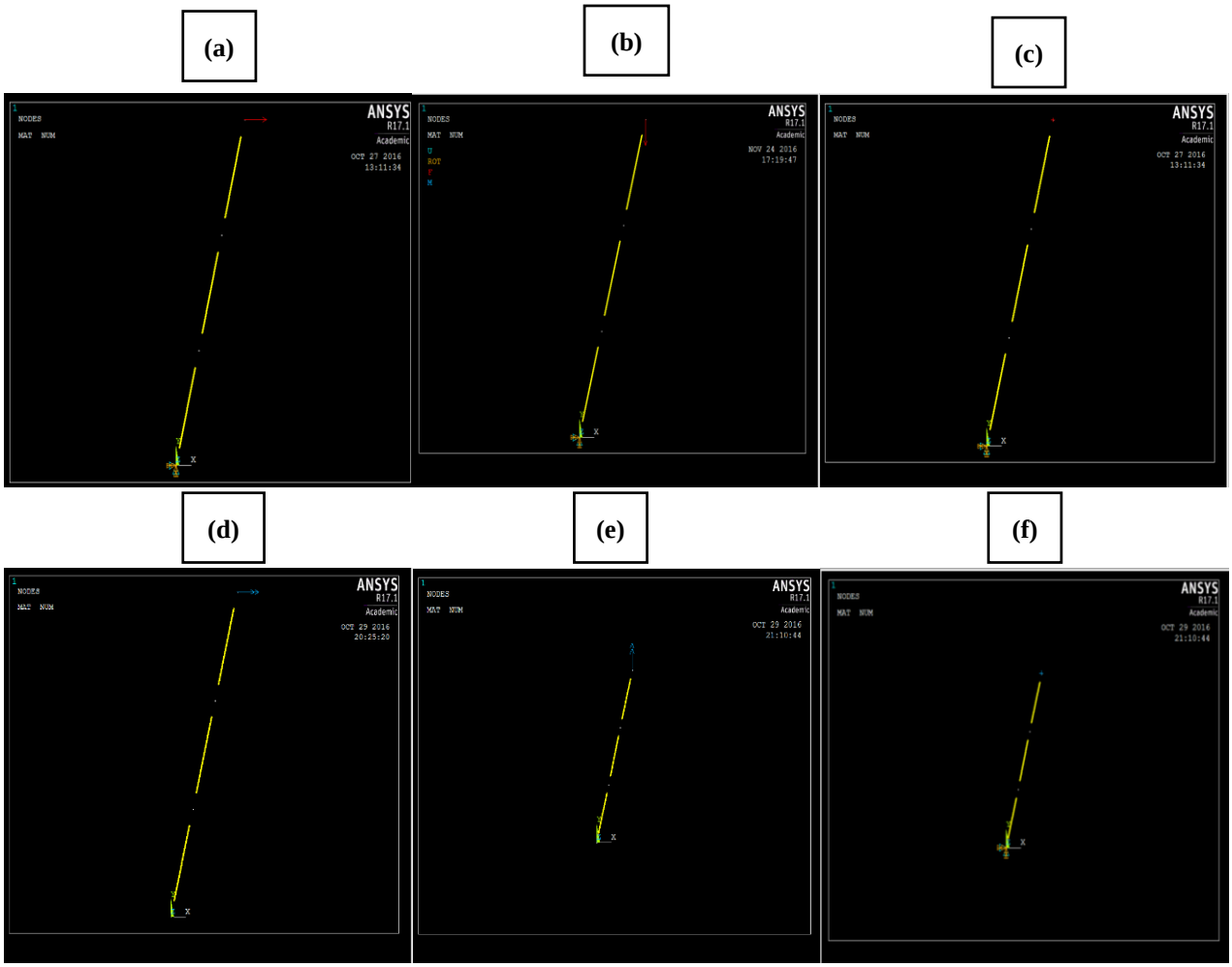

Figure 4.2 3-D frame element loaded at its free end in its 6 degrees of freedom. (a) Fx= 5nN (b) Fy= -5nN (c) Fz= 5nN (d) Mx= 5E-15N-m (e) My= 5E-15N-m (f) 5E-15N-m

Table 4.1 Results of model validation

ANSYS						
	Ux	Uy	Uz	θx	θy	θz
Fx	0.3943E-05	-0.985E-06	0.1266E-22	0.1829E-16	-0.4908E-17	-6.0438
Fy	0.9857E-06	-0.246E-06	0.3164E-23	0.4575E-16	-0.1227E-17	-1.5110
Fz	0.1267E-22	-0.316E-23	0.4189E-05	6.0438	-1.5110	-0.1953E-16
Mx	0.1829E-22	-0.458E-23	0.6044E-05	12.088	-0.425E-13	-0.3675E-16
My	-0.491E-23	0.1227E-23	-0.151E-05	-0.425E-13	12.088	0.9189E-17
Mz	-0.605E-05	0.1511E-05	-0.195E-22	-0.368E-16	0.9188E-17	12.088
Carbon Nanotube Model						
Fx	0.4021E-05	-1.005E-06	0	0	0	-6.0314
Fy	1.005E-06	-0.251E-06	0	0	0	-1.5078
Fz	0	0	0.4272E-05	6.031	-1.50784	0
Mx	0	0	0.6031E-05	12.062	0	0
My	0	0	-0.151E-05	0	12.0627	0
Mz	-0.603E-05	0.1508E-05	0	0	0	12.0627

Table 2.2 Model Percent Relative Error

Carbon Nanotube Model Percent Relative Error						
Fx	1.9%	1.9%	-	-	-	0.21%
Fy	1.9%	1.9%	-	-	-	0.21%
Fz	-	-	1.9%	0.21%	0.21%	-
Mx	-	-	0.21%	0.21%	-	-
My	-	-	0%	-	0.2%	-
Mz	0.3%	0.2%	-	-	-	0.2%

For the validation of the 3-D model kinematics, the commercial finite element program ANSYS was utilized. As shown in figure 4.2, a single spatial frame element was inclined such that it corresponds to a carbon nanotube contacting another nanotube. The free end of the spatial frame element is loaded with respect to all the six degrees of freedom and the corresponding displacement result is compared with those of our carbon nanotube model. The results are presented in tables 4.1 and 4.2 above where the percent differences are due to the fine mesh requirement of ANSYS. It must be noted that a scenario where ANSYS assumes that the single considered element is already discretized, will give a one to one equivalence in results with our model.

4.3 Results and Discussions

4.3.1 The effect of varied growth rates on the evolution of two carbon nanotubes and their reaction forces in the substrate.

A forest of two carbon nanotubes was first simulated to baseline the anticipated reaction forces from the interaction of carbon nanotubes. The aim is to better understand the effect

of growth rate mismatch between interacting carbon nanotubes and their resulting morphology. After the establishment of contact, the mismatch in growth rate will drive strain, deformation and the generation of reaction forces that evolve with time as the carbon nanotubes in contact deform. As an illustrative example, two carbon nanotubes with outer and inner radii of 20nm and 12nm were assigned growth rates of 50nm/time step and 55nm/time step respectively. The resulting carbon nanotube morphology, axial force, shear force, and bending moment are measured at the base of each carbon nanotube and presented in figures 4.3, 4.4 and 4.5 below. The carbon nanotubes were oriented such that they would contact and form van der Waals bond after sufficient time steps. After contact, the carbon nanotubes are then free to react and deform based upon the resulting forces and stiffness matrix that govern their deformation. Herein, emphasis was placed on the evaluation of the axial force transmitted to the base of each carbon nanotube as a result of interactions. It is at the base of carbon nanotubes that the active catalyst particle resides. Due to the wide application of the base growth method in the synthesis of carbon nanotube forests, the model is simulated using this approach where it is envisaged that the forces evaluated at the base of each carbon nanotube will be transmitted to the active catalyst particle.

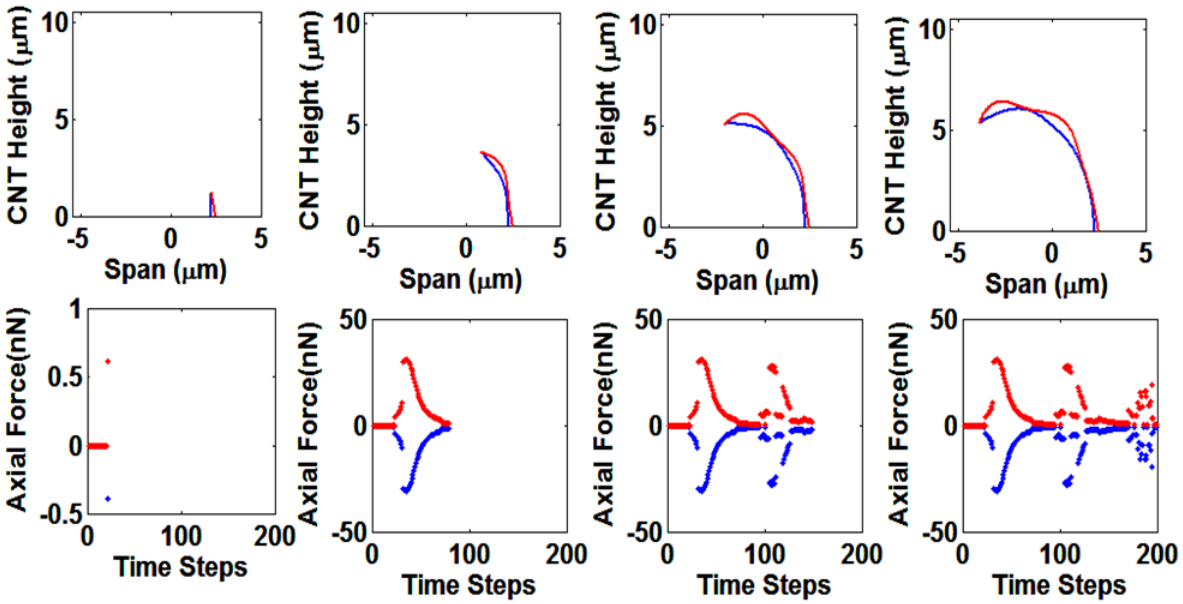

Figure 4.3 Morphology of two growing carbon nanotubes and their corresponding axial force.

The carbon nanotubes initially grow in a straight line towards each other until contact. Upon contact, the carbon nanotubes are locally bonded by van der Waals force. Subsequent time steps results in a mismatch in the lengthening below the point of contact, causing the carbon nanotubes to bow and curve in the direction of the slower growing tube. With continuous growth, additional contact points are established with time, and the carbon nanotubes continue to grow towards each other at their bases. The axial force imparted to the base of each carbon nanotube, as evaluated relative to the local coordinate system of each carbon nanotube, shows that the contact between tubes imparts load at the base of the carbon nanotube. For the simulated conditions as seen in figure 4.3, the magnitude of axial force is approximately 48nN. The slower growing carbon nanotube is pulled upward by the faster growing carbon nanotube, thereby imparting tensile (positive) loading. Conversely, the faster growing carbon nanotube is impeded by the slower growing carbon nanotube, imparting compressive (negative) loading at its base. The magnitude of the imparted axial force decays as the carbon nanotubes continue to grow and deform. Such

behavior is anticipated and may be approximated by the given model. It must be noted that the magnitude of axial forces expressed in figure 4.3 are not equal and opposite because forces are stated in the local coordinates relative to the orientation of each carbon nanotube. In global coordinates, the forces are balanced at all times.

The shear force and bending moment are also computed at every time step and are appropriately shown for completeness. Note that the shear force, as presented in figure 4.4 is transverse to the axial direction, and it is approximately 10x lower than the axial counterpart, though still significant. The magnitude of shear loading increases as contact points are established between the carbon nanotubes. With subsequent time steps after

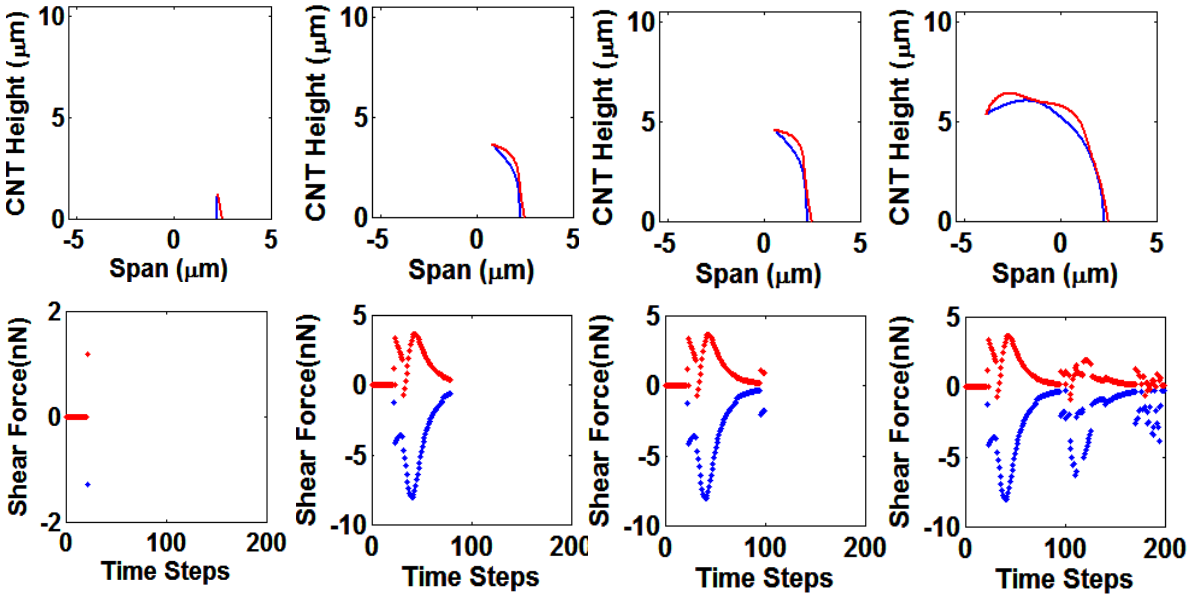

Figure 4.4 Morphology of two growing carbon nanotubes and their corresponding shear force.

contact, decay in the magnitude of shear force is seen as carbon nanotubes lengthen. This trend is very much consistent with that of the axial loading as seen in figure 4.3 above. It

must be noted that this shear force in an actual substrate would act to push/move catalyst particle along a substrate. The bending moment at the CNT bases follow similar temporal trends as the axial and shear force. Here, the bending moment maintains zero values for the first few time steps before contact. At contact, a sudden spike in the magnitude of the bending moment is noticed where the respective values for the fast and slow growing carbon nanotubes are largely in the positive range. As it was for axial and shear force, the following contacts after the initial contact is also characterized by an abrupt jump in the magnitude of bending moment. For the simulated conditions, the bending moment is in the order of 10^{-6} N-m. The observed results from the given plots are consistent with expected results from a simple linear 2-beam model where a small displacement is imparted on the faster growing carbon nanotube.

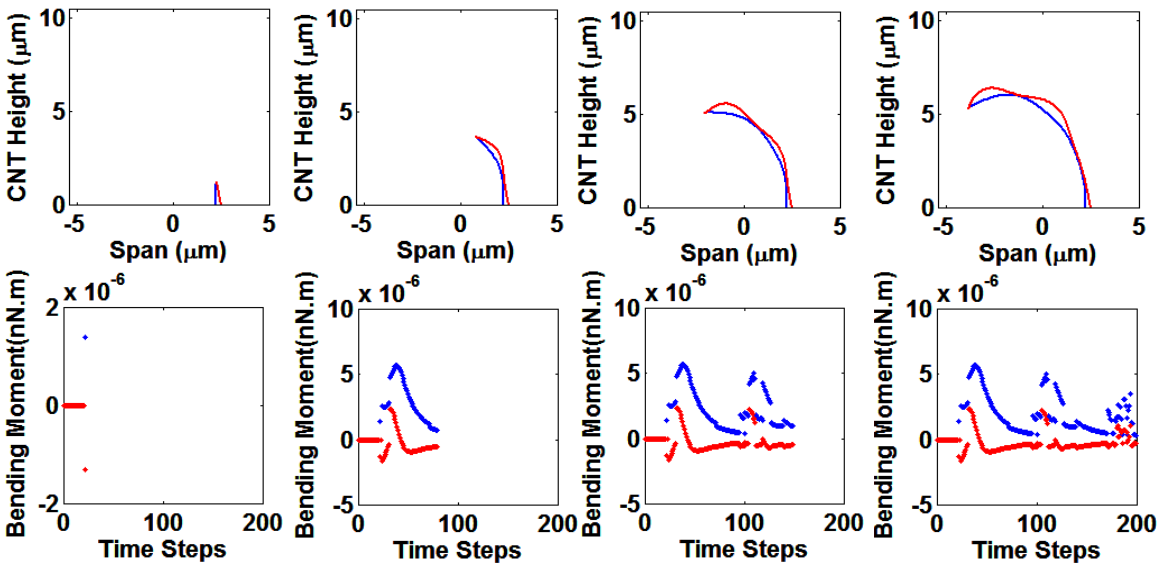

Figure 4.5 Morphology of two growing carbon nanotubes and their corresponding bending moment.

4.3.2 Effect of growth rate and diameter on the time averaged axial force in the substrate of a 2-D forest.

Having examined the loads generated within two carbon nanotube interactions, greater carbon nanotube populations were next examined. For the analysis of axial force in the substrate of a carbon nanotube forest, we considered a population of 100 carbon nanotubes grown for 200 time steps. The growth rate was given a Gaussian distributed growth rate with a standard deviation of 5% at an average of 65nm/step (figure 4.6). A uniform outer diameter of 5nm was employed for all tubes in the forest which were grown on a substrate of 15μm. In addition to this, the growth inclination angles of the nanotubes were distributed with a 5% standard deviation which ensures the desired interactions between nanotubes and leads to a tortuous forest. Similarly, a parallel study was embarked upon where the earlier parameters were maintained save for the diameter. In this case, a carbon nanotube forest with an outer diameter of 25nm was grown. To significantly reduce the margin of error in our numerical analysis, 20 exclusively different runs of the model was carried out whilst maintaining the basic physical parameters of the CNTs save for the growth rate.

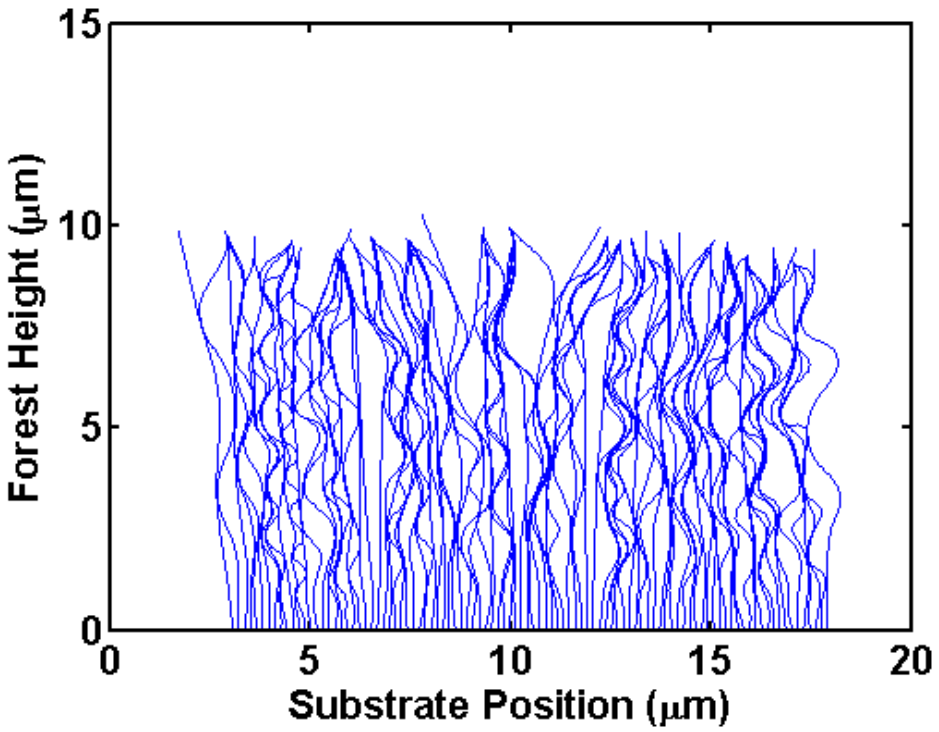

Figure 4.6 Morphology of a 100 carbon nanotube forest grown for 200 time steps.

This ensures diversity in rate distribution for each forest whilst maintaining the same values for all other parameters in the respective populations. Figure 4.7 are plots showing the trend between the time-averaged axial force and growth rate at the substrate of forest populations with 25nm and 5nm outer diameters respectively. The results show negative correlation between time-averaged axial force and growth rate. Also, the magnitude of the axial forces varies considerably with the outer diameters. Generally, an increase in the outer diameter of carbon nanotubes leads to an increase in the axial stiffness of the forest population. The stiffness of the carbon nanotube population which is an extensive property of the forest is dependent on geometry, area, and boundary conditions. Therefore, an increase in the outer diameter of carbon nanotubes translates to increase in their respective cross-sectional areas which leads to an increased forest stiffness which finally translates to increase in the values

of axial force. This relationship is due to the tendency of axial force scaling with respect to the bending stiffness. This is evident from a back-of-the-envelope calculation where axial force is seen to scale closer with respect to the moment of inertia as opposed to the area.

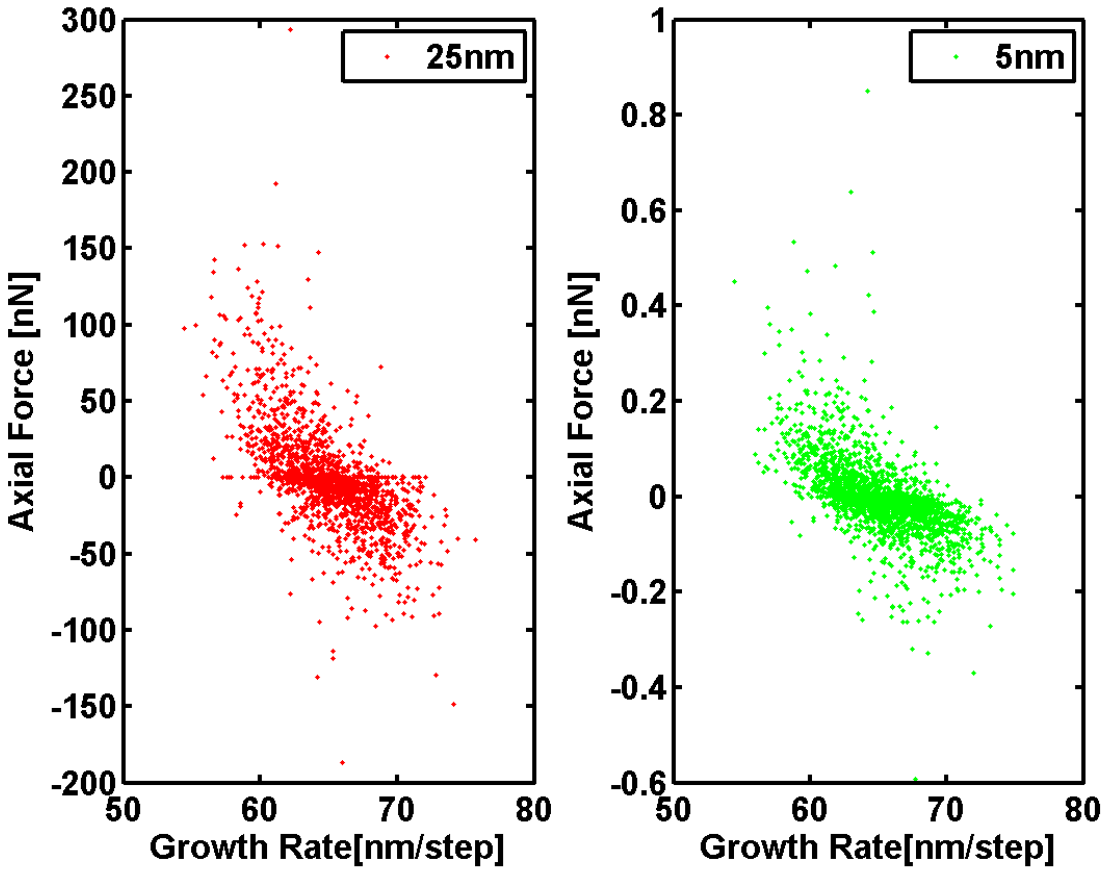

Figure 4.7 Growth rate dependence of axial force in the substrate of 5nm and 25nm diameter 2-D forests.

4.3.3 Effect of growth rate and diameter on the time averaged axial force in the substrate of a 3-D forest.

The transition from the 2-D to the 3-D model involves significant modification of the 2-D model since the physics of the problem becomes comparatively complex. For the3-D model, a spatial frame element is employed as presented in figure 4.1 above. Here, each node is allowed six degrees corresponding to displacements and rotations with respect to

the x, y and z axis. The previously employed scheme for the van der Waals force remains where bar elements are still utilized. As opposed to the 2-D model where the carbon nanotubes are restricted to the (x-y) plane, the 3-D model allows for relative freedom in all planes. The previous 2-D forest parameters like growth rate distribution, orientation angle, outer diameter, inner diameter, elastic modulus, average growth rate, average angular orientation are all carried into the 3-D model. These significant changes in the 3-D model as compared to the2-D case increases the computational cost greatly albeit the resulting plots bear a stronger similarity with scanning electron micrographs of actual carbon nanotube forests as seen in figures 4.8 and 4.9 below. Inherent forest phenomena like tortuosity, bundling, buckling and densification as observed in the 2-D model are also carried into the 3-D model although with better clarity.

For this study, two forest populations of 1600 nanotubes with respective outer diameters of 5nm and 25nm are grown for 200 time steps to elucidate the growth rate dependence of axial force at the substrate of a growing carbon nanotube forest. The forest tubes are grown at an average growth rate of 65nm/time step. In addition, the orientation angles of the forest population are grown at a mean value of 90° (normal to the substrate) where a standard deviation of 5° from the mean is implemented. Figure 4.8 below shows the resulting morphology of the forest.

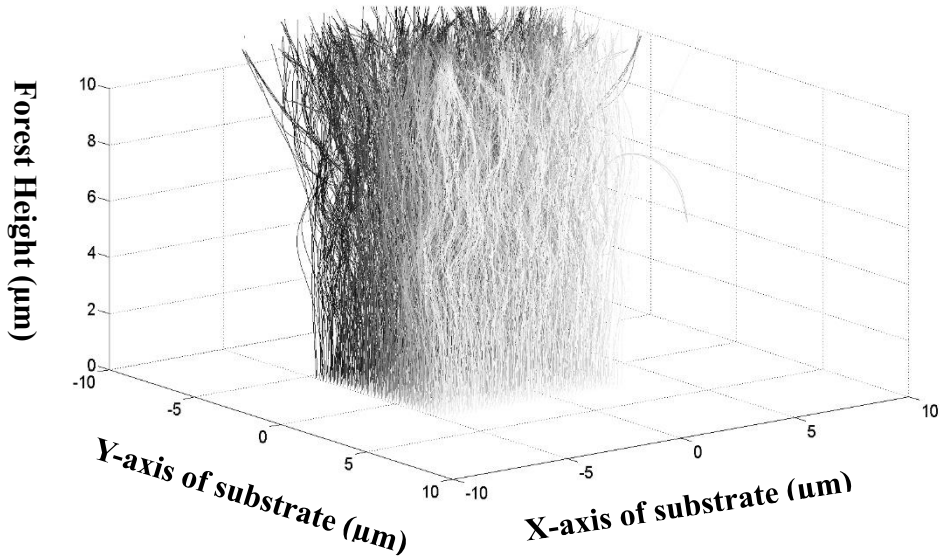

Figure 4.8 Morphology of a 3-Dimensional forest with 1600 nanotubes

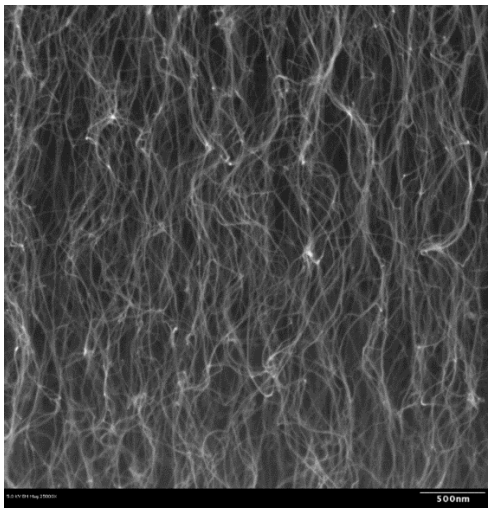

Figure 4.9 Morphology of an actual 3-D carbon nanotube forest.

The desire to elucidate the axial forces translated to the catalyst particles at the base of a carbon nanotube forest informs this study. The axial force evaluated per nanotube are relative to the local coordinate system since they allow for the simplest interpretation of

the active stress state in each element. As it was for the 2-D model, emphasis is placed on the examination of the elements located near the substrate since they are responsible for the transmission of the axial force impact on the forest substrate and catalyst particles. For the simulation sequence, the time-averaged axial force at the substrate of each nanotube is evaluated and recorded. This average over the duration of the growth sequence is plotted with the corresponding growth rate per nanotube and presented in figure 4.10 below.

Herein, the negative correlation between growth rate and time-averaged force transmitted to the substrate at the base of the nanotube as seen in the 2-D case of a growing carbon nanotube forest is maintained for the 3-D forest. From figure 4.10 below, it is observed that the magnitude of time averaged axial forces generally decreases with an increase in the magnitude of growth rate. Furthermore, a vivid correlation between the outer diameters and the resulting magnitude of time averaged axial forces can be noticed with the orders of magnitude remaining the same as it was for the 2-D case. The magnitude of axial force generally increases with any increase in the magnitude of the outer diameter of the forest tubes. Comparative analysis of the 2-D and 3-D forests show a discrepancy in the maximum and minimum values of axial forces. For the 2-D case, the forest shows axial force maximum values of approximately 290nN and 1nN for the forests with 25nm and 5nm outer diameters respectively. This is in contrast with the 3-D model that show maximum values of approximately 100nN and 0.15nN for the forests with 25nm and 5nm outer diameters respectively. This discrepancy is said to be due to the difference in the values of pitch in the respective forests. The 2-D forest was assigned a pitch value of 0.15μm whilst for the 3-D forest, the value was set at 0.2μm. This means that for the 2-D forest, the lower pitch value will significantly increase the propensity of interaction

between neighboring carbon nanotubes therefore increasing the axial load on nanotubes. In the case of the 3-D forest, the comparatively higher magnitude of pitch between the nanotubes means it requires further effort to establish interactions between carbon nanotubes and even a longer time to achieve a highly convoluted morphology. Also, it must be noted that for analysis in the 2-D model, the carbon nanotubes are artificially confined to a 2-D plane as opposed to the 3-D model that allows for bending and deformation in three dimensions. The comparatively lower tortuosity in the 3-D forest as opposed to the 2-D case means the loading on nanotubes is reduced therefore leading to lower values of axial force as seen in figure 4.10 below.

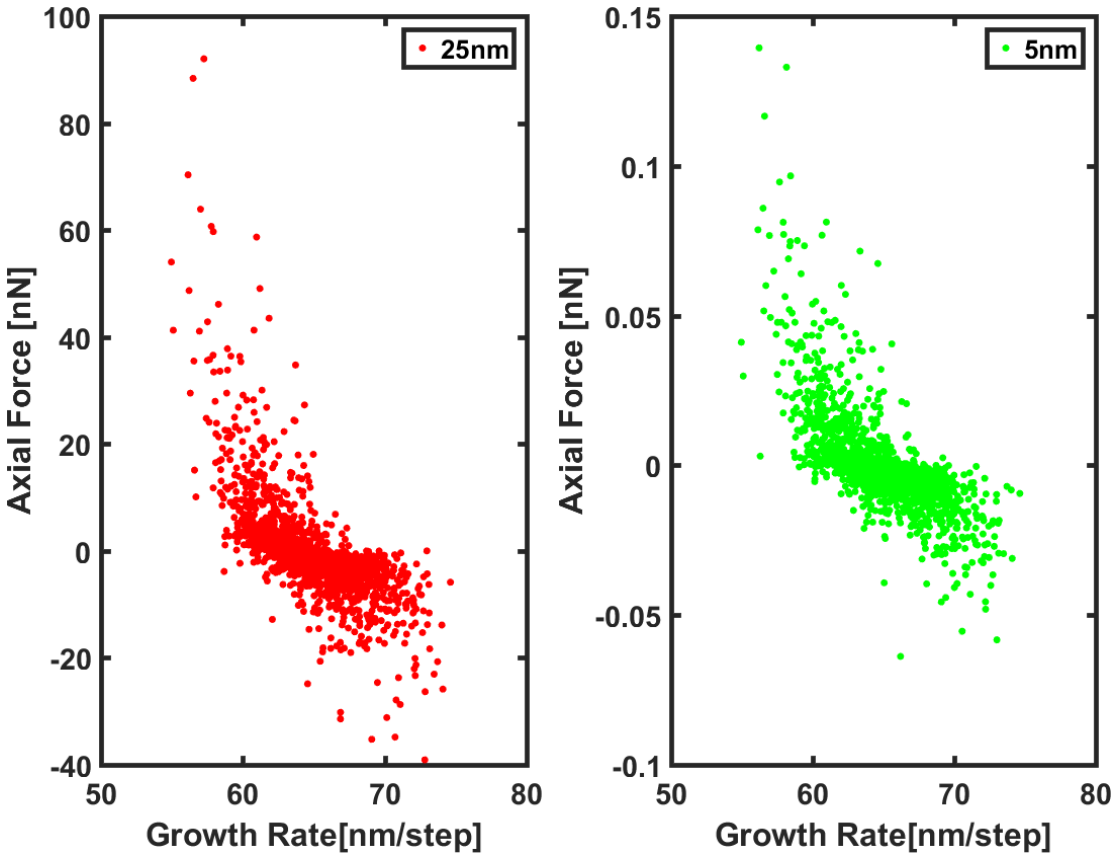

Figure 4.10 Growth rate dependence of axial force in the substrate of 5nm and 25nm diameter 3-D forests.

4.3.3 Effect of growth rate mismatch on the axial force in the substrate of a 3-D forest.

Due to the exceedingly great difficulty in quantifying the mismatch between contacting neighbors, the analysis herein takes an approach that considers a pair-wise growth rate mismatch. In this approach, consideration is given to the nodes of individual nanotubes which are closest to the substrate and at the same time in contact with nodes from neighboring tubes. Here, the growth rate mismatch relative to the contacting tubes are evaluated and this entails the subtraction of their respective rate values. Carbon nanotubes that have nodes that are in contact with more than one node and at the same time closest to the substrate are neglected in order to simplify the analysis**.** After computation of the growth rate mismatch, the corresponding axial force mismatch at the substrate for the contacting nodes are evaluated and plotted to examine the resulting trends. It must be noted that the loads are not the product of pair-wise interactions alone but are also due to their distribution amongst nanotubes in the forest.

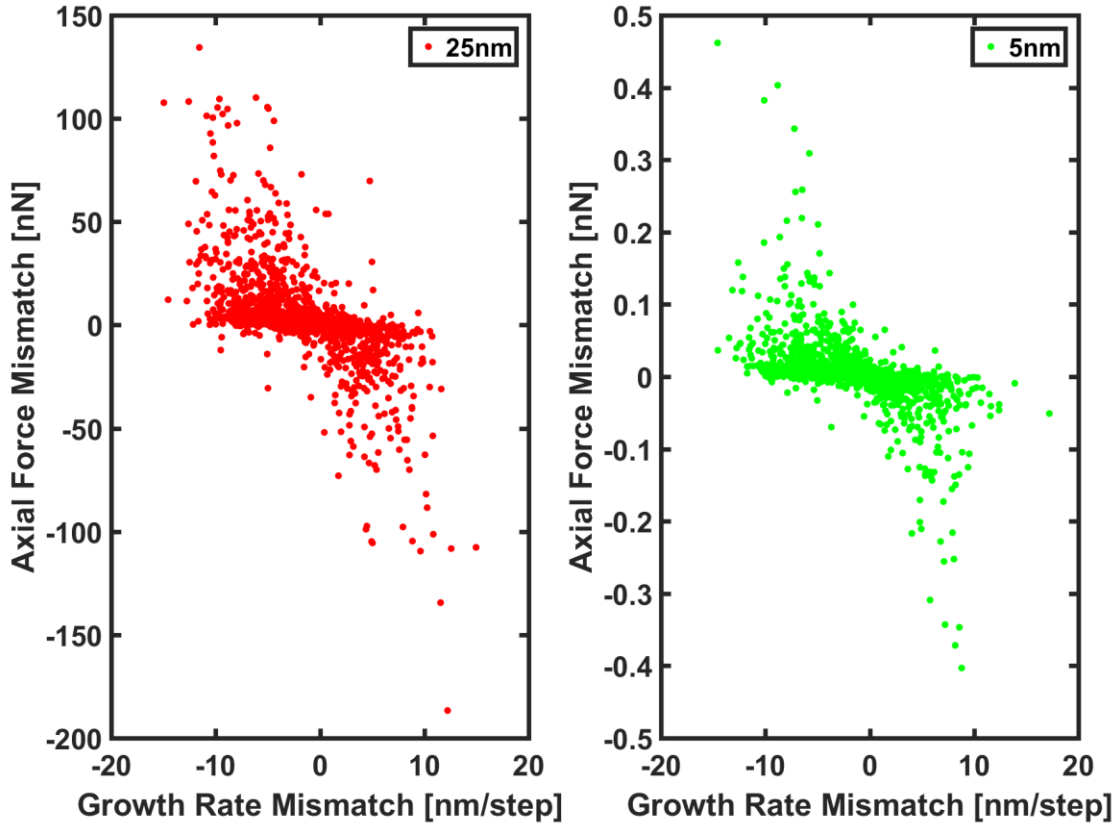

Figure 4.11 Relationship between axial force mismatch and growth rate mismatch at the substrate of a growing 3-D carbon nanotube forest.

The plot in figure 4.11 show a consistent trend with earlier data in figures 4.9 and 4.10 therefore serving as an excellent validation tool for our results. The trend can be said to be linear where the axial force match is said to decrease with an increase in the value of the axial force mismatch. Also, from the plot it could be gleaned that the faster growing carbon nanotubes tend to be in a state of compression as evidenced by their corresponding axial force mismatch. The consequence of this seemingly minute forces is magnified when they are thought of in terms of unit length. In this sense, the resulting pressure on the catalyst surface and particles become humongous. This is noticed by the movement of catalyst particles and their pulling away from the substrate or even their total alteration in size. Any

form of alteration of the catalytic particle could be due to strain energy changing the activation energy required to diffuse carbon from the gas phase to solid carbon which is incorporated into the carbon nanotubes. In a removed distance from the catalyst particle, these forces/pressures may be adequate to cause kinking amongst the forest carbon nanotubes. This is an area that has not been considered and could be embarked upon for future work.

4.4 Conclusion

A comprehensive analysis of the mechanical behavior of a growing carbon nanotube forest has been presented. The growth and mechanical deformation of a carbon nanotube forest are simulated using a finite element model. The model plots show strong consistency with experimental results where forest phenomena like buckling, bundling, and densification et cetera can be observed.

A simplified model of a two-nanotube forest is shown whilst investigating the inherent mechanics in the forest. The two-nanotube forest helped presage the interactions in a fully grown nanotube population. The resulting plots shows that in addition to growth rate, the slower growing carbon nanotubes play a key role in determining the forest morphology. The slower tubes tend to act as inhibitors to the faster tubes whilst existing in a state of perpetual tension for a significant portion of the growth sequence. The faster growing tubes whilst following the lead of the slower growing carbon nanotubes tend to exist in a state of compression where buckling is also prevalent in their parts.

Extensive work is presented on the time averaged axial force present in the substrate of a 2-D and 3-D carbon nanotube forest. Here, a linear correlation between the time averaged axial force and growth rate is observed. The time averaged axial load in the forest generally decreases at the substrate with increasing growth rate. This modeling result could potentially serve as an effective tool for delamination, buckling, bundling and densification prediction in real carbon nanotube forests.

Lastly, the growth rate mismatch between contacting carbon nanotubes at the substrate is observed to understand its effect on the corresponding axial force mismatch. Here, the linear trend as seen for the time averaged axial force and growth rate plot is observed. This intrinsic trend of the forest serves as some sort of validation of our forest.

Chapter 5 Conclusion and Future Work

5.1 Conclusion

The employed finite element model was shown to be a viable tool for the study of growing carbon nanotube forests. The model results show strong consistency with actual carbon nanotube forests whilst maintaing all forest phenomena like buckling, bundling, densification, crusting et cetera.

The parametric study on the model proved that diverse population morphologies could be obtained by varying forest parameters like growth rate, outer diameter and angular orientation. Herein it was established that the curvature of the tortuous carbon nanotubes generally decrease with an increase in the diameter of carbon nanotubes. The increase in carbon nanotubes diameter also translates to an increase in the forest height due to reduced tortuosity. Also, through the model it was established that variation of the orientation angles of nanotubes gives some sort of control over the time of contact between forest nanotubes. Furthermore, the growth rate parameter was shown to take precedence over the other parameters of the forest, therefore becoming the main driving force behind most forest phenomena.

Analysis of loading at the substrate of a forest population indicates that the slowest growing carbon nanotube will be in a state of perpetual tension after establishment of contact with other population tubes. On the other hand, the fastest growing carbon nanotube showed the opposite by undergoing compression upon contact with other tubes. Also, this compressive forces was showed to decay to neutral loadings with subsequent growth steps.

Presented also is the higly complex 3-D model that represents the closest to an actual carbon nanotube population as seen in the literature. Herein, forest phenomena has seen in

2-D seamlessly translates into 3-D with an even clearer depiction of forest morphology. Analysis of the effects of growth rate mismatch on the substrate was embarked upon with results showing a linear trend between force mismatch at the substrate and growth rate mismatch. The analysis of substrate axial force in 3-D was carried out where the resulting data also showed consistency with those of 2-D.

5.2 Future Work

Potential areas of interest could be electrical, thermal, electronic and vibration analyses of growing carbon nanotube forests. The model could also be redesigned to accommodate the mass of individual carbon nanotubes thereby incorporating the system mass matrix. Another potential route of interest could be the incorporation of material non-linearity which will essentially widen the scope of the model. Also, it must be noted that the modeling construct can potentially be used to interrogate forest properties after the growth phase of simulation is complete.

References

[1] W.D. Callister, D.G. Rethwisch, Materials science and engineering: an introduction, Wiley New York2007.
[2] G. Lalwani, A.M. Henslee, B. Farshid, L. Lin, F.K. Kasper, Y.-X. Qin, A.G. Mikos, B. Sitharaman, Two-dimensional nanostructure-reinforced biodegradable polymeric nanocomposites for bone tissue engineering, Biomacromolecules 14(3) (2013) 900-909.
[3] C. De las Casas, W. Li, A review of application of carbon nanotubes for lithium ion battery anode material, Journal of Power Sources 208 (2012) 74-85.
[4] M.F. De Volder, S.H. Tawfick, R.H. Baughman, A.J. Hart, Carbon nanotubes: present and future commercial applications, Science 339(6119) (2013) 535-9.
[5] E.T. Thostenson, Z. Ren, T.-W. Chou, Advances in the science and technology of carbon nanotubes and their composites: a review, Composites science and technology 61(13) (2001) 1899-1912.
[6] K. Banerjee, S. Im, N. Srivastava, Can Carbon Nanotubes Extend the Lifetime of On-Chip Electrical Interconnections?, 2006 1st International Conference on Nano-Networks and Workshops, IEEE, 2006, pp. 1-9.
[7] J. Li, Q. Ye, A. Cassell, H.T. Ng, R. Stevens, J. Han, M. Meyyappan, Bottom-up approach for carbon nanotube interconnects, Applied Physics Letters 82(15) (2003) 2491-2493.
[8] P.G. Collins, M.S. Arnold, P. Avouris, Engineering carbon nanotubes and nanotube circuits using electrical breakdown, science 292(5517) (2001) 706-709.
[9] H.W.C. Postma, T. Teepen, Z. Yao, M. Grifoni, C. Dekker, Carbon nanotube single-electron transistors at room temperature, Science 293(5527) (2001) 76-79.
[10] P. Cherukuri, S.M. Bachilo, S.H. Litovsky, R.B. Weisman, Near-infrared fluorescence microscopy of single-walled carbon nanotubes in phagocytic cells, Journal of the American Chemical Society 126(48) (2004) 15638-15639.
[11] R.B. Weisman, S.M. Bachilo, Dependence of optical transition energies on structure for single-walled carbon nanotubes in aqueous suspension: an empirical Kataura plot, Nano Letters 3(9) (2003) 1235-1238.
[12] S.-H. Jhi, Y.-K. Kwon, K. Bradley, J.-C.P. Gabriel, Hydrogen storage by physisorption: beyond carbon, Solid state communications 129(12) (2004) 769-773.
[13] A. Jones, T. Bekkedahl, C. Kiang, Storage of hydrogen in single-walled carbon nanotubes, Nature 386 (1997) 377.
[14] Z. Li, V.P. Kunets, V. Saini, Y. Xu, E. Dervishi, G.J. Salamo, A.R. Biris, A.S. Biris, Light-harvesting using high density p-type single wall carbon nanotube/n-type silicon heterojunctions, Acs Nano 3(6) (2009) 1407-1414.
[15] K. Kordas, G. Tóth, P. Moilanen, M. Kumpumäki, J. Vähäkangas, A. Uusimäki, R. Vajtai, P. Ajayan, Chip cooling with integrated carbon nanotube microfin architectures, Applied Physics Letters 90(12) (2007) 123105.
[16] S. Iijima, Helical microtubules of graphitic carbon, nature 354(6348) (1991) 56-58.
[17] L. Radushkevich, V. Lukyanovich, O strukture ugleroda, obrazujucegosja pri termiceskom razlozenii okisi ugleroda na zeleznom kontakte, Zurn Fisic Chim 26(1) (1952) 88-95.

[18] M. Monthioux, V.L. Kuznetsov, Who should be given the credit for the discovery of carbon nanotubes?, Carbon 44(9) (2006) 1621-1623.
[19] H.-S.P. Wong, D. Akinwande, Carbon nanotube and graphene device physics, Cambridge University Press2011.
[20] G. Overney, W. Zhong, D. Tomanek, Structural rigidity and low frequency vibrational modes of long carbon tubules, Zeitschrift für Physik D Atoms, Molecules and Clusters 27(1) (1993) 93-96.
[21] S. Iijima, C. Brabec, A. Maiti, J. Bernholc, Structural flexibility of carbon nanotubes, The Journal of chemical physics 104(5) (1996) 2089-2092.
[22] L. Vaccarini, C. Goze, L. Henrard, E. Hernandez, P. Bernier, A. Rubio, Mechanical and electronic properties of carbon and boron–nitride nanotubes, Carbon 38(11) (2000) 1681-1690.
[23] J. Bernholc, C. Brabec, M. Buongiorno Nardelli, A. Maiti, C. Roland, B. Yakobson, Theory of growth and mechanical properties of nanotubes, Applied Physics A: Materials Science & Processing 67(1) (1998) 39-46.
[24] B. Yakobson, G. Samsonidze, G. Samsonidze, Atomistic theory of mechanical relaxation in fullerene nanotubes, Carbon 38(11) (2000) 1675-1680.
[25] N. Hu, Z. Masuda, C. Yan, G. Yamamoto, H. Fukunaga, T. Hashida, The electrical properties of polymer nanocomposites with carbon nanotube fillers, Nanotechnology 19(21) (2008) 215701.
[26] J. Che, T. Cagin, W.A. Goddard III, Thermal conductivity of carbon nanotubes, Nanotechnology 11(2) (2000) 65.
[27] M. De Folder, S. Tawfick, R. Baughman, A. Hart, Carbon nanotubes: present and future applications, Science 339 (2013) 535-539.
[28] T. Kashiwagi, F. Du, J.F. Douglas, K.I. Winey, R.H. Harris, J.R. Shields, Nanoparticle networks reduce the flammability of polymer nanocomposites, Nature materials 4(12) (2005) 928-933.
[29] A. Beigbeder, P. Degee, S.L. Conlan, R.J. Mutton, A.S. Clare, M.E. Pettitt, M.E. Callow, J.A. Callow, P. Dubois, Preparation and characterisation of silicone-based coatings filled with carbon nanotubes and natural sepiolite and their application as marine fouling-release coatings, Biofouling 24(4) (2008) 291-302.
[30] Z. Wu, Z. Chen, X. Du, J.M. Logan, J. Sippel, M. Nikolou, K. Kamaras, J.R. Reynolds, D.B. Tanner, A.F. Hebard, Transparent, conductive carbon nanotube films, Science 305(5688) (2004) 1273-1276.
[31] S.Y. Hong, G. Tobias, K.T. Al-Jamal, B. Ballesteros, H. Ali-Boucetta, S. Lozano-Perez, P.D. Nellist, R.B. Sim, C. Finucane, S.J. Mather, Filled and glycosylated carbon nanotubes for in vivo radioemitter localization and imaging, Nature materials 9(6) (2010) 485-490.
[32] A. Bianco, K. Kostarelos, M. Prato, Making carbon nanotubes biocompatible and biodegradable, Chemical communications 47(37) (2011) 10182-10188.
[33] J.H. Hafner, C.L. Cheung, C.M. Lieber, Growth of nanotubes for probe microscopy tips, Nature 398(6730) (1999) 761-762.
[34] S.S. Wong, E. Joselevich, A.T. Woolley, C.L. Cheung, C.M. Lieber, Covalently functionalized nanotubes as nanometre-sized probes in chemistry and biology, Nature 394(6688) (1998) 52-55.

[35] H. Sugie, M. Tanemura, V. Filip, K. Iwata, K. Takahashi, F. Okuyama, Carbon nanotubes as electron source in an x-ray tube, Applied Physics Letters 78(17) (2001) 2578-2580.
[36] M. Park, B.A. Cola, T. Siegmund, J. Xu, M.R. Maschmann, T.S. Fisher, H. Kim, Effects of a carbon nanotube layer on electrical contact resistance between copper substrates, Nanotechnology 17(9) (2006) 2294.
[37] S. Vollebregt, F. Tichelaar, H. Schellevis, C. Beenakker, R. Ishihara, Carbon nanotube vertical interconnects fabricated at temperatures as low as 350 c, Carbon 71 (2014) 249-256.
[38] B.A. Cola, J. Xu, C. Cheng, X. Xu, T.S. Fisher, H. Hu, Photoacoustic characterization of carbon nanotube array thermal interfaces, Journal of applied physics 101(5) (2007) 054313.
[39] T. Yamada, Y. Hayamizu, Y. Yamamoto, Y. Yomogida, A. Izadi-Najafabadi, D.N. Futaba, K. Hata, A stretchable carbon nanotube strain sensor for human-motion detection, Nature nanotechnology 6(5) (2011) 296-301.
[40] M.R. Maschmann, G.J. Ehlert, B.T. Dickinson, D.M. Phillips, C.W. Ray, G.W. Reich, J.W. Baur, Bioinspired Carbon Nanotube Fuzzy Fiber Hair Sensor for Air-Flow Detection, Advanced Materials 26(20) (2014) 3230-3234.
[41] A. Cao, P.L. Dickrell, W.G. Sawyer, M.N. Ghasemi-Nejhad, P.M. Ajayan, Super-compressible foamlike carbon nanotube films, Science 310(5752) (2005) 1307-1310.
[42] M.R. Maschmann, Q. Zhang, R. Wheeler, F. Du, L. Dai, J. Baur, In situ SEM observation of column-like and foam-like CNT array nanoindentation, ACS applied materials & interfaces 3(3) (2011) 648-653.
[43] S.B. Hutchens, A. Needleman, J.R. Greer, Analysis of uniaxial compression of vertically aligned carbon nanotubes, Journal of the Mechanics and Physics of Solids 59(10) (2011) 2227-2237.
[44] M. Bedewy, A.J. Hart, Mechanical coupling limits the density and quality of self-organized carbon nanotube growth, Nanoscale 5(7) (2013) 2928-2937.
[45] Y. Gao, T. Kodama, Y. Won, S. Dogbe, L. Pan, K.E. Goodson, Impact of nanotube density and alignment on the elastic modulus near the top and base surfaces of aligned multi-walled carbon nanotube films, Carbon 50(10) (2012) 3789-3798.
[46] M. Bedewy, E.R. Meshot, H. Guo, E.A. Verploegen, W. Lu, A.J. Hart, Collective mechanism for the evolution and self-termination of vertically aligned carbon nanotube growth, The Journal of Physical Chemistry C 113(48) (2009) 20576-20582.
[47] M. Bedewy, E.R. Meshot, M.J. Reinker, A.J. Hart, Population growth dynamics of carbon nanotubes, ACS nano 5(11) (2011) 8974-8989.
[48] C.P. Deck, J. Flowers, G.S. McKee, K. Vecchio, Mechanical behavior of ultralong multiwalled carbon nanotube mats, Journal of Applied Physics 101(2) (2007) 023512.
[49] M.R. Maschmann, G.J. Ehlert, S. Tawfick, A.J. Hart, J.W. Baur, Continuum analysis of carbon nanotube array buckling enabled by anisotropic elastic measurements and modeling, Carbon 66 (2014) 377-386.
[50] M. Xu, D.N. Futaba, M. Yumura, K. Hata, Alignment control of carbon nanotube forest from random to nearly perfectly aligned by utilizing the crowding effect, Acs Nano 6(7) (2012) 5837-5844.
[51] J. Xu, T.S. Fisher, Enhancement of thermal interface materials with carbon nanotube arrays, International Journal of Heat and Mass Transfer 49(9) (2006) 1658-1666.

[52] C. Li, E.T. Thostenson, T.-W. Chou, Sensors and actuators based on carbon nanotubes and their composites: a review, Composites Science and Technology 68(6) (2008) 1227-1249.
[53] A. Bianco, K. Kostarelos, M. Prato, Applications of carbon nanotubes in drug delivery, Current opinion in chemical biology 9(6) (2005) 674-679.
[54] R.H. Chan, C.K. Fung, W.J. Li, Rapid assembly of carbon nanotubes for nanosensing by dielectrophoretic force, Nanotechnology 15(10) (2004) S672.
[55] F. Kreupl, A.P. Graham, G. Duesberg, W. Steinhögl, M. Liebau, E. Unger, W. Hönlein, Carbon nanotubes in interconnect applications, Microelectronic Engineering 64(1) (2002) 399-408.
[56] M.R. Maschmann, Integrated simulation of active carbon nanotube forest growth and mechanical compression, Carbon 86 (2015) 26-37.
[57] Y. Won, Y. Gao, M.A. Panzer, R. Xiang, S. Maruyama, T.W. Kenny, W. Cai, K.E. Goodson, Zipping, entanglement, and the elastic modulus of aligned single-walled carbon nanotube films, Proceedings of the National Academy of Sciences 110(51) (2013) 20426-20430.
[58] S.S. Rao, The finite element method in engineering, Elsevier2010.